

**KARADENİZ TECHNICAL UNIVERSITY  
THE GRADUATE SCHOOL OF NATURAL AND APPLIED SCIENCES**

**DEPARTMENT OF MINING ENGINEERING**

**ANALYSIS OF ROCK FATIGUE IN TUNNELS BY FINITE ELEMENT METHOD**



**MASTER'S THESIS**

**by Manuel Diego ROMERO VASQUEZ**

**AUGUST 2021  
TRABZON**



**KARADENİZ TECHNICAL UNIVERSITY  
THE GRADUATE SCHOOL OF NATURAL AND APPLIED SCIENCES**

**DEPARTMENT OF MINING ENGINEERING**

**ANALYSYS OF ROCK FATIGUE IN TUNNELS BY FINITE ELEMENT METHOD**

**Manuel Diego ROMERO VASQUEZ**

**This thesis is accepted to give the degree of  
"MASTER OF SCIENCE"**

**By  
The Graduate School of Natural and Applied Sciences at  
Karadeniz Technical University**

**The Date of Submission : 25 / 06 / 2021**

**The Date of Examination : 03 / 08 / 2021**

**Supervisor : Prof. Dr. Kerim AYDINER**

**Trabzon 2021**

## **PREFACE**

The realization of this research involved multiple debts of gratitude. In particular, I would like to extend my sincere gratitude to Prof. Kerim AYDINER, who provided patient advice and guidance throughout the research process.

From those who gave me their trust and shared their knowledge with me, I have special gratitude for two excellent people: Res. Asst. Melek HANIM, and Res. Asst. Serkan İNAL. Furthermore, I would like to express my special thanks to the faculty members of the Mining Engineering Department of KTU.

I conclude by thanking my family for believing and give me unconditional support. Just three words to my grandmother "we did it".

Manuel Diego ROMERO VASQUEZ

Trabzon 2021

## **DECLARATION**

I declare that this thesis entitled “ANALYSIS OF THE ROCK FATIGUE IN TUNNELS BY FINITE ELEMENT METHOD” is original research. It is written by me and has not been submitted to any previous university or published in any institution. I confirm that the work submitted is my own work, except for the different data and information from other publications, which has been cited in the reference section. My own contribution and that of the other authors have been adequately indicated and mentioned in this work.  
03/08/2021.



Manuel Diego ROMERO VASQUEZ

## TABLE OF CONTENTS

	<u>Page No</u>
PREFACE.....	III
DECLARATION.....	IV
TABLE OF CONTENTS .....	V
ÖZET .....	VII
SUMMARY .....	VIII
LIST OF FIGURES .....	IX
LIST OF TABLES .....	XI
LIST OF SYMBOLS.....	XII
1. INTRODUCTION .....	1
1.1. Overview.....	1
1.2. Literature Review .....	2
1.3. Aim and Objectives .....	5
1.4. Thesis Structure .....	6
2. MATERIALS AND METHODS .....	8
2.1. Characterization of Rock Samples.....	8
2.2. Laboratory Tests .....	9
2.2.1. Physico-Mechanical Properties of Bayburt Tuff .....	10
2.2.1.1. Density Test.....	10
2.2.1.2. Determination of Porosity and Void Ratio .....	12
2.2.1.3. Uniaxial Compressive Strength Test .....	13
2.2.1.4. Young's Modulus and Poisson's Ratio .....	17
2.2.1.5. Brazilian Tensile Strength (BTS) Test .....	20
2.2.2. Cyclic Loading Test.....	22
2.2.2.1. Cyclic Loading Test Methodology on Bayburt Tuff .....	24
3. NUMERICAL SIMULATION BY FEM.....	30
3.1. Introduction to Finite Element Method .....	30
3.1.1. Basic Principles of the Finite Element Method .....	31

3.1.1.1.	Analysis Stages By PLAXIS 3D .....	32
3.2.	Bayburt Tuff Fatigue Analysis Under PLAXIS 3D .....	35
3.2.1.	Hoek-Brown Failure Criterion.....	35
3.2.1.1.	The Rock Mass Young's Modulus ( $E_{rm}$ ) .....	36
3.2.1.2.	Intact Rock Parameter ( $M_i$ ).....	37
3.2.1.3.	Dilatancy ( $\Psi$ ) and $\Sigma_\psi$ .....	37
3.2.1.4.	Geological Strength Index (GSI) .....	38
3.2.1.5.	Disturbance Factor (D) .....	39
3.2.2.	Excavation of a Hypothetical NATM Tunnel .....	41
3.2.3.	Stage 1: Geometry .....	42
3.2.3.1.1.	Definition of Boundary Conditions and Material Properties.....	42
3.2.3.1.2.	Definition of NATM Tunnel Profile.....	46
3.2.3.2.	Stage 2: Mesh Generation.....	47
3.2.3.3.	Stage 3 and 4: Performing Calculations and Viewing the Results .....	48
4.	DISCUSSION OF RESULTS .....	59
4.1.	Comparative Analysis of the Loading Scenarios by Results.....	59
4.1.1.	$ u_{max} $ Assessment .....	59
4.1.2.	$\Sigma_3$ Assessment.....	60
4.1.3.	SF Assessment.....	61
5.	CONCLUSIONS .....	64
6.	REFERENCES .....	65
7.	ANNEXES.....	69

BIOGRAPHY

Yüksek Lisans

## ÖZET

### TÜNELLERDE KAYA YORULMASININ SONLU ELEMANLAR YÖNTEMİ KULLANILARAK ANALIZI

Manuel Diego ROMERO VASQUEZ

Karadeniz Teknik Üniversitesi  
Fen Bilimleri Enstitüsü  
Maden Mühendisliği Anabilim Dalı  
Danışman: Prof. Dr. Kerim AYDINER  
2021, 68 Sayfa, 8 Sayfa Ek

Bu tez, yeraltı açıklıkları etrafındaki deformasyon gelişimi üzerinde döngüsel yüklemenin neden olduğu yorulma etkisini araştırmaktadır. Bayburt Tüfö içinde NATM yöntemi ile açılacak bir varsayımsal tünelin analizi için PLAXIS 3D yazılımı kullanılarak analizler gerçekleştirilmiştir. Çalışma iki aşamada gerçekleştirilmiştir: 1) kaya özelliklerinin fiziko-mekanik karakterizasyonu ve statik ve döngüsel yükleme testlerinin gerçekleştirilmesi ve 2) statik ve döngüsel yükleme durumları için sayısal analizlerin gerçekleştirilmesi. Sayısal analizlerde Hoek-Brown yenilme kriterleri kullanılarak 4 farklı tünel modeli kullanılmıştır. Yorulma modellerinde frekans değişimi (0,2, 0,6 ve 1,0 Hz) simüle edilirken, tekrar sayısı (500 tekrar) ve yükleme genliği (kayaç statik kırılma yükünün 30-50 %si) sabit tutulmuştur. Sonuçlar, i) frekans Bayburt tufünün dayanım ve elastisite değerlerini doğrudan etkilemiştir; başka bir deyişle, kaya numunesi üzerindeki yorulma etkileri daha düşük frekanslarda önemli boyutlarda gerçekleşmiştir, ii) statik yüklemeye oranla tekrarlı yüklemelerde daha düşük yer değiştirmeler gözlenmiştir ( $|u_{max}| (0.2 \text{ Hz}) < |u_{max}| (0.6 \text{ Hz}) < |u_{max}| (1.0 \text{ Hz}) < |u_{max}| (\text{statik})$ ), iii) minimum asal gerilme ( $\sigma_3$ ) ve frekans arasında negatif bir ilişki bulunmuştur, iv) yorulma modellerinde frekans ve emniyet katsayısı (SF) arasında doğrusal ilişki gözlenmiştir.

**Anahtar Sözcükler:** Yorulma, tekrarlı Yükleme, Tünelcilik, Yeni Avusturya Tünelcilik Yöntemi (NATM), PLXIS 3D, Sonlu Elemanlar Yöntemi

Master Thesis

## SUMMARY

### ANALYSIS OF THE ROCK FATIGUE IN TUNNELS BY FINITE ELEMENT METHOD

Manuel Diego ROMERO VASQUEZ

Karadeniz Technical University  
The Graduate School of Natural and Applied Sciences  
Mining Engineering Graduate Program  
Supervisor: Prof. Dr. Kerim AYDINER  
2021, 68 Pages, 8 Pages Appendix

This thesis investigates the fatigue effect caused by cyclic loading on the deformation development around the underground openings. Employing PLAXIS 3D FEM package for the numerical modelling of a hypothetical tunnel opened by the NATM in Bayburt Tuff for static and cyclic loading conditions to analyze stresses and deformation developments. The investigation is divided into two stages: 1) physico-mechanical characterization of rock properties and performance of static and cyclic loading tests, and 2) numerical analysis applied to static and cyclic loading case. PLAXIS 3D simulated four hypothetical NATM tunnels considering the Hoek-Brown failure criterion; being three of them based only on frequency variation (0.2 Hz, 0.6 Hz, and 1.0 Hz) while keeping the number of cycles (500) and load amplitude (30-50% from UCS) constant. Concluding as follow: i) the frequency directly influences the strength and elasticity values of the Bayburt tuff; in other words, the fatigue effects on rock specimen will be significant at lower frequencies. ii)  $|u_{\max}|$  (0.2 Hz)  $< |u_{\max}|$  (0.6 Hz)  $< |u_{\max}|$  (1.0 Hz)  $< |u_{\max}|$  (static), being  $|u_{\max}|$  the maximum total displacement. iii) tuff responds with an inverse relationship between principal stresses and frequency. iv) the fatigue effect influence appears through proportionality between frequency and safety factor (SF) values.

**Key Words:** Fatigue, Cyclic loading, Tunneling, New Austrian Tunnelling Method (NATM), PLAXIS 3D, Finite Element Method (FEM).



## LIST OF FIGURES

	<u>Page No</u>
Figure 1.1. Thesis structure .....	7
Figure 2.1. Flowchart for the development of the experiments.....	9
Figure 2.2. Laboratory work flow chart .....	10
Figure 2.3. Physical measurements from Bayburt tuff specimens .....	11
Figure 2.4. Stress-strain curve in geomaterials (H Wang et al., 2010).....	14
Figure 2.5. UCS test for Bayburt tuff specimens .....	15
Figure 2.6. Rock specimens exhibit a shear failure with conjugates.....	16
Figure 2.7. Bayburt tuff arrangement for elasticity test .....	18
Figure 2.8. Tuff specimen subjected to the elasticity test .....	18
Figure 2.9. Stress-strain curve for static loads case in the range of 5% - 95% .....	19
Figure 2.10. Brazilian or indirect tensile strength test.....	20
Figure 2.11. BTS test for Bayburt tuff specimens .....	20
Figure 2.12. Bayburt tuff failure mode after BTS tests .....	22
Figure 2.13. Stress-strain curve (a) of Liaoning tuff, and (b) of Brisbane tuff .....	24
Figure 2.14. Flow chart for the cyclic loading tests .....	25
Figure 2.15. Bayburt tuff specimen subjected to UCS and cyclic loading test.....	27
Figure 2.16. Cyclic loading distribution for specimen UF 1-1 (0.2 Hz) .....	27
Figure 2.17. UCS curve after cyclic loading test for specimen UF 1-1 (0.2 Hz) .....	28
Figure 2.18. Stress-strain curve and cyclic loading test for specimen UF 1-3 (0.2 Hz).....	28
Figure 3.1. Two ways to solve a problem .....	30
Figure 3.2. Continuum model.....	32
Figure 3.3. Parts of a discretized model .....	32
Figure 3.4. Problem analysis stages by PLAXIS 3D Finite Element Software .....	33
Figure 3.5. The finite element meshing process.....	34
Figure 3.6. Problem solving process by PLAXIS 3D Finite Element Software .....	35
Figure 3.7. Hoek-Brown failure parameters.....	36
Figure 3.8. Basic GSI chart (Hoek and Marinos, 2000) .....	39

Figure 3.9. Front and three-dimensional view of Bayburt tuff block.....	42
Figure 3.10. NATM tunnel profile, adapted from Plaxis (2018).....	46
Figure 3.11. Three-dimensional NATM tunnel sequencing phase by phase .....	47
Figure 3.12. Generated mesh for Bayburt tuff block.....	48
Figure 3.13. Total displacements by phase for static loading case.....	49
Figure 3.14. Total displacements by phase for cyclic loading case (0.2 Hz) .....	50
Figure 3.15. Total displacements by phase for cyclic loading case (0.6 Hz) .....	51
Figure 3.16. Total displacements by phase for cyclic loading case (1.0 Hz) .....	52
Figure 3.17. Principal stresses by phase for static loading case .....	53
Figure 3.18. Principal stresses by phase for cyclic loading case (0.2 Hz).....	54
Figure 3.19. Principal stresses by phase for cyclic loading case (0.6 Hz).....	55
Figure 3.20. Principal stresses by phase for cyclic loading case (1.0 Hz).....	56
Figure 3.21. Safety factor curves for static and cyclic loading cases .....	57
Figure 4.1. Stress distribution acting on the tunnel profile .....	59
Figure 4.2. Maximum total displacements ( $ u_{max} $ ) per phase and scenario [mm] .....	60
Figure 4.3. Maximum and minimum principal stresses per phase and scenario [kN/m <sup>2</sup> ]...	61
Figure 4.4. Safety factor (SF) per phase and scenario.....	62
Figure 4.5. Scenario comparison based on $\sigma_{ci}$ and E .....	63

## LIST OF TABLES

	<u>Page No</u>
Table 2.1. Densities of Bayburt tuff specimens.....	12
Table 2.2. Volume of void space, porosity, and void ratio of Bayburt tuff specimens.....	13
Table 2.3. Stages of the stress-strain curve in geomaterials (Wang et al., 2010).....	14
Table 2.4. UCS test results applied to Bayburt tuff specimens in their natural state .....	15
Table 2.5. Engineering classification for intact rock (Deere and Miller, 1966).....	16
Table 2.6. Young's modulus for Bayburt tuff for static loading case .....	19
Table 2.7. BTS test results applied to tuff specimens in their natural state.....	21
Table 2.8. Input parameters for cyclic loading tests.....	26
Table 2.9. Output parameters after cyclic and static loading tests .....	29
Table 3.1. Mandatory parameters in FEM.....	31
Table 3.2. Guidelines for estimating disturbance factor (D) .....	40
Table 3.3. Input parameters requested by PLAXIS 3D Finite Element Software.....	43
Table 3.4. Material properties of the Bayburt tuff (static case).....	44
Table 3.5. Material properties of the Bayburt tuff (cyclic case, 0.2 Hz).....	44
Table 3.6. Material properties of the Bayburt tuff (cyclic case, 0.6 Hz).....	45
Table 3.7. Material properties of the Bayburt tuff (cyclic case, 1.0 Hz).....	45
Table 3.8. Summary of the maximum total displacements, $ u_{max} $ , units in mm .....	58
Table 3.9. Summary of the principal total stresses, $\sigma_3$ , units in $kN/m^2$ .....	58
Table 3. 10. Safety factors for static and cyclic loading scenarios.....	58

## LIST OF SYMBOLS

**NATM:** New Australian Tunneling Method

**FEM:** Finite Element Method.

**UCS:** Uniaxial Compressive Strength.

**BTS:** Brazilian Tensile Strength

**$\Sigma_{ci}$ :** Uniaxial compressive strength of the intact rock.

**E:** Young's modulus.

**$|\mathbf{u}_{\max}|$ :** Maximum total displacements.

**$\sigma_3$ :** Radial stresses.

**SF:** Safety factor

# 1. INTRODUCTION

## 1.1. Overview

Rocks in their natural location are regularly subjected to static and dynamic loads, which differ in how much the rock changes when it has been under loads in time intervals. Dynamic loading is commonly encountered due to shocks, blasting, high-speed trains, etc. (Cerfontaine and Collin, 2017) and, under these conditions, the rock suffers a degradation or progressive fatigue due to the application of cyclic loads, causing the modification of its internal structure that over time and if the loads are sufficiently high the rock will enter a state of rupture. A rupture refers to the failure process whereby a structure disintegrates into two or more pieces (B. Shen et al., 2014).

The fatigue phenomenon plays an essential role in designing all the structural elements that make up an underground rock excavation, and the laboratory tests are the starting point for the study of this phenomenon. Singh (1989) performed a series of cyclic loading tests on graywacke rock specimens to find their fatigue and strain hardening behaviours, concluding an inverse relationship between stress amplitude and fatigue life of rock and proportionality between strain hardening percentage and the number of loads. Beşer and Aydiner (2018) subjected Tephrite samples to different cycles (50, 100, 150, and 200) under constant amplitude and frequency to evaluate the effect produced by the loading cycles on the compressive strength of the rock samples concluding in an inverse relationship between the number of cycles and the compressive strength of the rock. In other words, Tephrite strength reduces with increasing the number of cycles, thus revealing fatigue strength is affected by the number of cycles in cyclic compression conditions. Wang et al. (2014) subdued granite specimens to cyclic loading tests under triaxial compression conditions to analyze the hydro-mechanical behaviour of a storage facility by FEM. After that, they implemented a constitutive model to understand how fatigue behaves under the mean stress effect; moreover, the simulation of cases synchronous and asynchronous storage and extraction of crude oil in the facility. The simulation results denoted a threshold for fatigue failure because there is a stress level arising from the transition from volumetric compaction to volumetric dilatation, the crown settlement and plastic deformation in the asynchronous case were lesser

than those in the synchronous case, as well as the volume of groundwater inflow inside the caverns in the asynchronous case was greater than that in the synchronous case.

The investigation trends invite us to go beyond laboratory outcomes analysis and develop simulations by computer. Since the numerical methods have gained considerable importance in designing the underground openings, FEM appears as a useful prediction tool to calculate stresses and displacements in tunnels (Gunter et al., 1994). In other words, FEM allows simulating the behaviour that an underground structure will have throughout its construction stage; however, it is essential to compare simulation results with obtained measurements from monitoring the tunnels over a long period (Boidy et al., 2002; Pellet, 2009). The literature offers interesting research regarding FEM use, such as the case of underground openings design analysis. For example, Fasihnikoutalab et al. (2012) make models to analyze both settlement and stability design factors from Line-4 Tehran, Iran subway employing PLAXIS 8.2 finite element software. FEM is a useful tool to assess the rockburst phenomena, as revealed by the investigations conducted by Manoucherian and Cai (2017), whose objective is to quantify the influence of geological weak planes on rockburst occurrence in tunnels subjected to static load increase and dynamic disturbance by Abaqus<sup>2D</sup>.

## **1.2. Literature Review**

Analysis of the effect of rock fatigue using the numerical methods is employing as a part of the underground opening design; research shows that the results from fatigue cyclic tests provide high value-added at the moment to design by numerical methods (For instance, Wang et al., 2014; and Demir, Özbayır, 2016). Moreover, academics such as Sing, 1988; and Bagdevand and Petroš, 2005 make considerable contributions to the rock fatigue subject.

Fasihnikoutalab et al. (2012) started with two of the most critical tunneling factors: settlement and stability, and how numerical modeling techniques approach them for analysis. One of these techniques is FEM that analyzes tunnel stability and predicts the ground movement. Their study uses PLAXIS 8.2 finite element software to analyze the stability and settlement of Line – 4 Tehran, Iran subway, and simulate tunnel behaviour, consisting of both soil and rock layers. After both design and meshing for the tunnel, it proceeded with the calculations in two phases. The first phase with the soil layer active and tunnel support tools inactive without any replacement or deformation; and the second phase with an active support system but the soil layer inside the tunnel inactivated. Finally, the conclusions were

the following: (i) according to the calculated lining thickness, a thickness of 35 cm was optimum for the coverage system. (ii) based on the analysis, the most displacements obtained in the ceiling and floor were equal to  $9.65 \cdot 10^{-3}$  m. (iii) the main-stress computed in the model with the lining was  $-478 \text{ kN/m}^2$ . (iv) the stress returned to normal status for a distance of 13 m since the tunnel center.

Wang et al. (2014) analyzed the hydro-mechanical behaviour of an underground crude oil storage facility in granite, subject to cyclic loading during its operation, by FEM. Their research consisted of laboratory experiments to study granite's fatigue behaviour subjected to cyclic loading tests under triaxial compression conditions. As a result of the tests mentioned above, the threshold for fatigue failure is defined, which refers to the stress generated by the transition from volumetric compaction to volumetric dilation. Likewise, the research defined parameters such as a linear elastic model, a yield surface, an associated flow rule, and a kinematic hardening model. These parameters will be inputs for the simulation by finite elements regarding the synchronous and asynchronous storage and extraction of crude oil in the facility. The simulations for synchronous and asynchronous cases show the following conclusions: the evaluation of crown settlement and plastic deformation shows the synchronous case was more significant than the asynchronous case. The volume of groundwater inflow into the cavern's analysis, the synchronous case was less than the asynchronous case. An important point to keep in mind is that both synchronous and asynchronous cases regarding the stability and containment properties of the caverns remained adequate during the operation phase.

Solans et al. (2015) compares the seismic response of NATM tunnels in Santiago's soft soil through the seismic distortion method of soil-applied in structural analysis software and a finite difference software for soil-structure interaction. Additionally, for the last case, a seismic record has been applied. Three numerical analyses by different kinds of methodologies were carried out: modeling through FEM by SAP 2000 software (Case I), the second and third cases have been carried out with Finite Difference Models for soil-structure interaction by FLAC 3D software. The comparison parameters were the coating thickness of the tunnel structural analysis; for the Case I: 75 cm, Case II: 70 cm, and Case III: 60 cm. In conclusion, the thicknesses determined based on the results of the differences that do not exceed 25%; however, regarding each method's complexity and execution times, it was found that Case III > Case II > Case I.

Demir K and Özbayır T (2016) were responsible for the Eurasia Tunnel Project's design and development. Their project consisted of the twin NATM tunnels constructed across the Trakya Formation, characterized by a fragile and weathered rock mass sections; moreover, a detail to take into account is that the twin tunnels were passing under a populous district, city water lines, and public buildings with a minimum of 8 m to a maximum of 41 m overburden. Urban tunnel design both took into account the lining stresses and ground deformations to be concerned, and to the design process, the following steps were taken: (1) site investigation and laboratory tests, (2) excavation geometry and supports, (3) mesh, (4) material model, (5) model validation, (6) 2D numerical model, and (7) 3D numerical model. Simulating the twin tunnels by FEM, the authors performed the monitoring and back analysis of each phase of the project. Finally, the researchers concluded that (i) geotechnical methods do not represent an exact way to model the ground behaviour; in light of this, an understanding of the tunnel geology and the system behaviour could be a good option. (ii) both Mohr-Coulomb and hardening soil models may provide accurate results for predicting the surface settlements and tunnel deformations. (iii) numerical models performed could be used not only for the design stage but also for the construction stage to verify.

Considering the role played by discontinuities around tunnel boundaries to trigger the rockburst phenomenon, Manoucherian and Cai (2017) develop a methodology for rockburst analysis. Based on the results, there was a significant increase in velocity and released kinetic energy of failed rocks, a larger fault zone around the tunnel, and a mesh with significant deformation for models with discontinuities; consequently, rock failure with the last type of model was more violent. Finally, the modelling results validate those geological structures close to deep excavations may be one relevant factor for developing the rockbursts.

Singh (1988) worked with Graywacke specimens from the Flagstaff Formation, that rock specimens were subject to cyclic loads tests to analyze both fatigue and strain hardening rock intact behaviours. First of all, the author obtained a UCS average of 185 MPa that will be a part of the fatigue test inputs. To carry out the fatigue tests were defined input parameters such as predefined stresses, frequency, and a predetermined number of cycles to determine the following conclusions: (i) it was defined fatigue stress of 87% of UCS average. (ii) based on the S-N curves, the stress amplitude has an inverse relationship with the number of cycles to failure. (iii) assuming a maximum applied stress, stress amplitude, and cyclic frequency, the percentage strain hardening is directly related to the number of load cycles.



(iv) the increment of the maximum applied stress also increases the percentage in strain hardening.

Bagde and Petroš studied the rock behaviour and rock mass inside the excavation system subjected to uniaxial cyclic loading by evaluating of the effect of loading waveform and amplitude on the fatigue behaviour of intact sandstone by laboratory tests. These tests consisted of two experiment sets; in the first one, the sinusoidal, ramp, and square waveforms has been performed with a peak amplitude of 0.05 mm and loading frequency of 5 Hz; and in the last one, the test has been conducted at a range of amplitudes from 0.05 to 0.3 mm at a frequency of 5 Hz using sinusoidal and ramp waveforms. Deriving the following conclusions: (i) the maximum loading rate in a waveform has strongly influenced the damage accumulation in rock; on the other hand, the type of loading waveform affects the various rock properties in uniaxial cyclic loading conditions. (ii) the rock failure mechanism is a function of loading waveform and amplitude; consequently, the amplitude has a great significance in cyclic loading conditions.

To analyze the effect of static and dynamic disturbances on rockbursts, Su et al. (2018) performed rockbursts tests induced by ramp and cyclic dynamic disturbances under triaxial conditions, where the ramp dynamic disturbance's strain rate was  $5 \times 10^{-3}$  Hz, whereas the other was between  $2 \times 10^{-3}$ - $5 \times 10^{-3}$  Hz. The results confirm that both the ramp and dynamic disturbances induce rockbursts, and this is evidenced by the kinetic energy of the ejected fragments behaviour: (i) in the ramp dynamic disturbance case, the strength of the specimen, and the kinetic energy ejected fragments first increase and then decrease. (ii) while in the cyclic dynamic disturbance case, the ejected fragments' kinetic energy first increases and then decreases proportionally to the cyclic dynamic disturbance frequency increase. (iii) there is just one process of violent fragment ejection in the failure process of rockburst induced by the dynamic ramp disturbance, while for the cyclic dynamic disturbance scenario, there are several ejections. (iv) different trends of damage evolution of rocks between the ramp and cyclic dynamic disturbance. (v) the energy mechanisms of rockbursts induced by both ramp and cyclic dynamic disturbance are different.

### **1.3. Aim and Objectives**

This research aims to analyze the stability of a tunnel with cyclic loading history under static loading conditions; for this purpose, hypothetical tunnel, considering just frequency changes, is modeled by the PLAXIS 3D FEM package in a Bayburt tuff environment under

NATM. The findings of this thesis are expected to accord importance to the fatigue effect caused by cyclic loading on the development of deformation around underground openings; to achieve this, the following objectives are established:

- i. To determine the physico-mechanical properties of Bayburt tuff specimens.
- ii. To analyze rock behaviour of Bayburt tuff under frequency changes.
- iii. To model a hypothetical NATM tunnel design using PLAXIS 3D finite element software for static and cyclic loading scenarios and obtaining stability parameters such as total displacements, principal total stresses, and safety factors for each loading case.
- iv. To assess how the effect of fatigue affects the design of NATM tunnels through the stability parameters analysis for each cyclic load scenario.

#### **1.4. Thesis Structure**

The thesis consists of five chapters: Chapter 1 gives an overall picture of the subject under study and mentions the relevant past studies. Chapter 2 focuses on determining the physico-mechanical properties of the Bayburt tuff and the performance of the cyclic loading tests. Chapter 3 simulates hypothetical NATM tunnel design scenarios for both static and cyclic loads cases. Chapter 4 compares the results of both scenarios to discuss the effect of the frequency for the cyclic loading case. In the end, Chapter 5 briefly describes the research given in this thesis. Figure 1.1 shows the structure and interconnection of chapters.

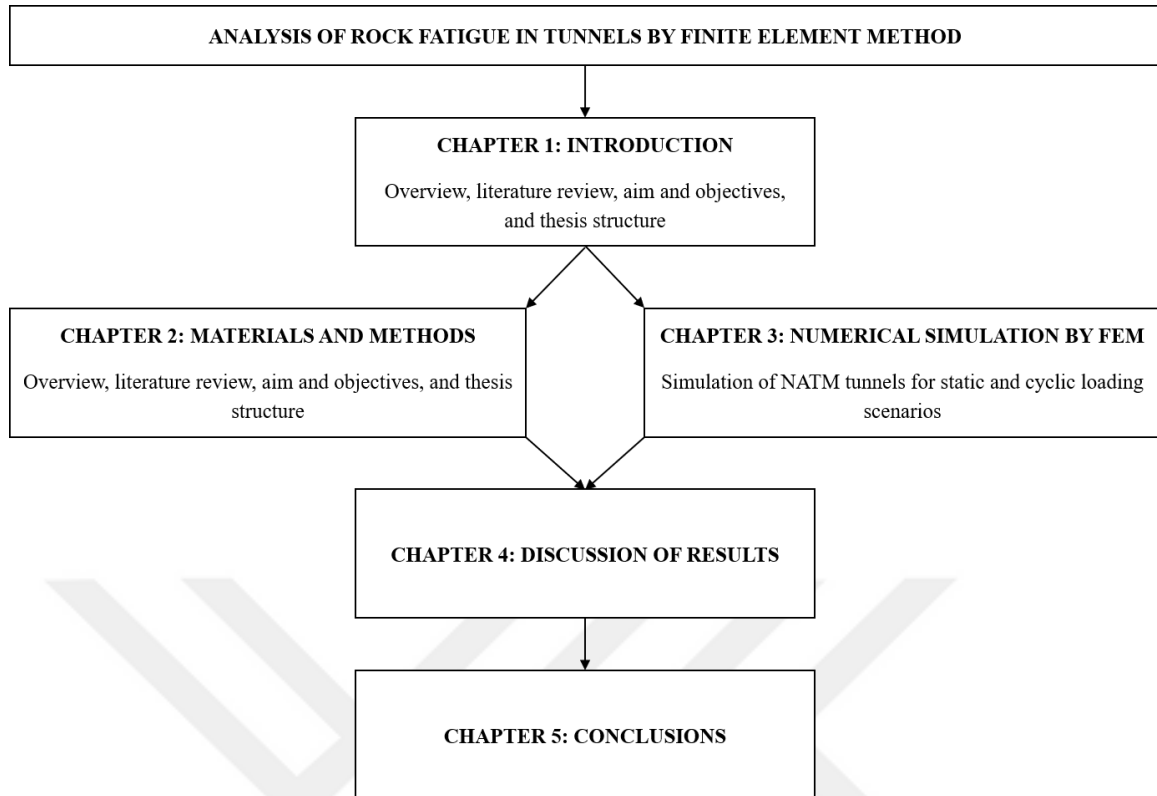


Figure 1.1. Thesis structure

In this thesis, the effect of rock fatigue for a hypothetical NATM tunnel designed in Bayburt tuff mass subjected to static and cyclic loading scenarios is analyzed using PLAXIS 3D finite element software. In chapter 2, the real data is obtained through rock laboratory tests for both static and cyclic loading conditions. In chapter 3, static and cyclic loading scenarios for a NATM tunnel are simulated by PLAXIS 3D finite element software, then analyze the tunnel stability output parameters that are: total displacements, radial stresses, and safety factor for each loading case. Only the loading frequency change for the cyclic loading conditions is simulated to analyze the effect of the far-field and near-field blast in the tunneling process. The differences between total displacements, radial stresses, and safety factors for each scenario are discussed by Chapter 4. Finally, the relevant conclusions from this thesis are embodied in Chapter 5.

## **2. MATERIALS AND METHODS**

### **2.1. Characterization of Rock Samples**

Figure 2.1 develops the flowchart concerning the laboratory works stage and consists of four steps. Below is a brief description of the four stages mentioned:

- i. The first stage intended to describe the most relevant intrinsic properties of the Bayburt tuff, such as the mineralogic and petrographic analysis.
- ii. The second stage describes the standards proposed by the ISRM to prepare the Bayburt tuff samples for both static and cyclic loads tests.
- iii. The third stage refers to define the physico-mechanical properties of Bayburt tuff, such as density, unit volume weight, apparent porosity, and void ratio, and the performance of static loads tests, such as UCS, BTS, and Young's modulus tests.
- iv. The fourth stage stands for analyzing the fatigue effect's influence in Bayburt tuff samples subjected to cyclic loads at different frequencies through load versus time graphs, calculating the uniaxial strength after cyclic loads, and then carrying out the UCS and elasticity tests.

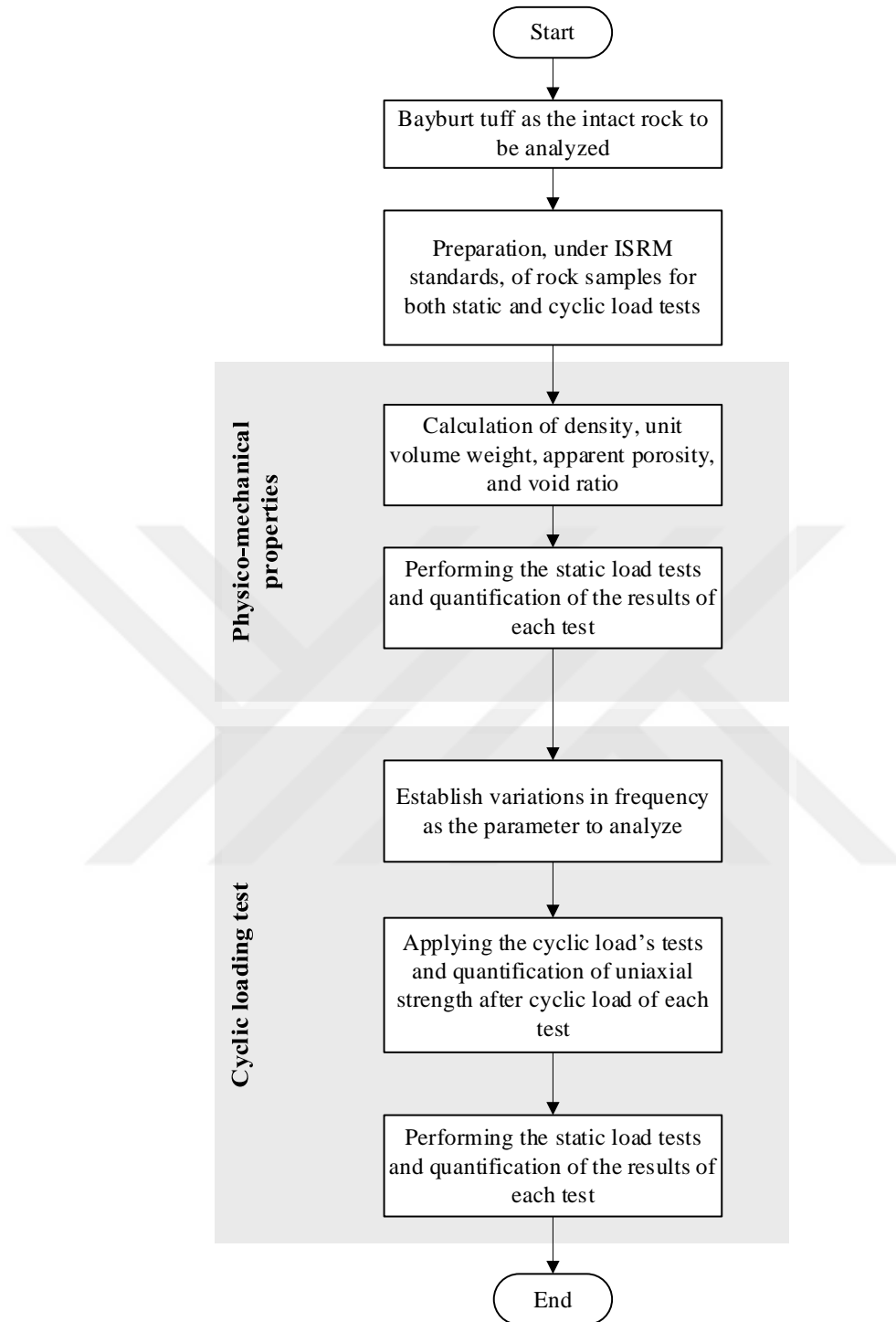


Figure 2.1. Flowchart for the development of the experiments

## 2.2. Laboratory Tests

The rock subject to study is the Bayburt tuff, whose intact rock samples were obtained from a private company. The performance of the laboratory work develops in seven phases

described in Figure 2.2 and mentioned below: 1) prepare samples for core drilling; 2) core drilling; 3) taking the specimen; 4) core inspection; 5) specimen cutting / grinding end surface flatness / parallelism; 6) final inspection; and 7) specimen ready for the uniaxial load tests.

A detailed highlight is that all the tuff specimens were prepared considering the guidelines and standards suggested by ISRM (2017).

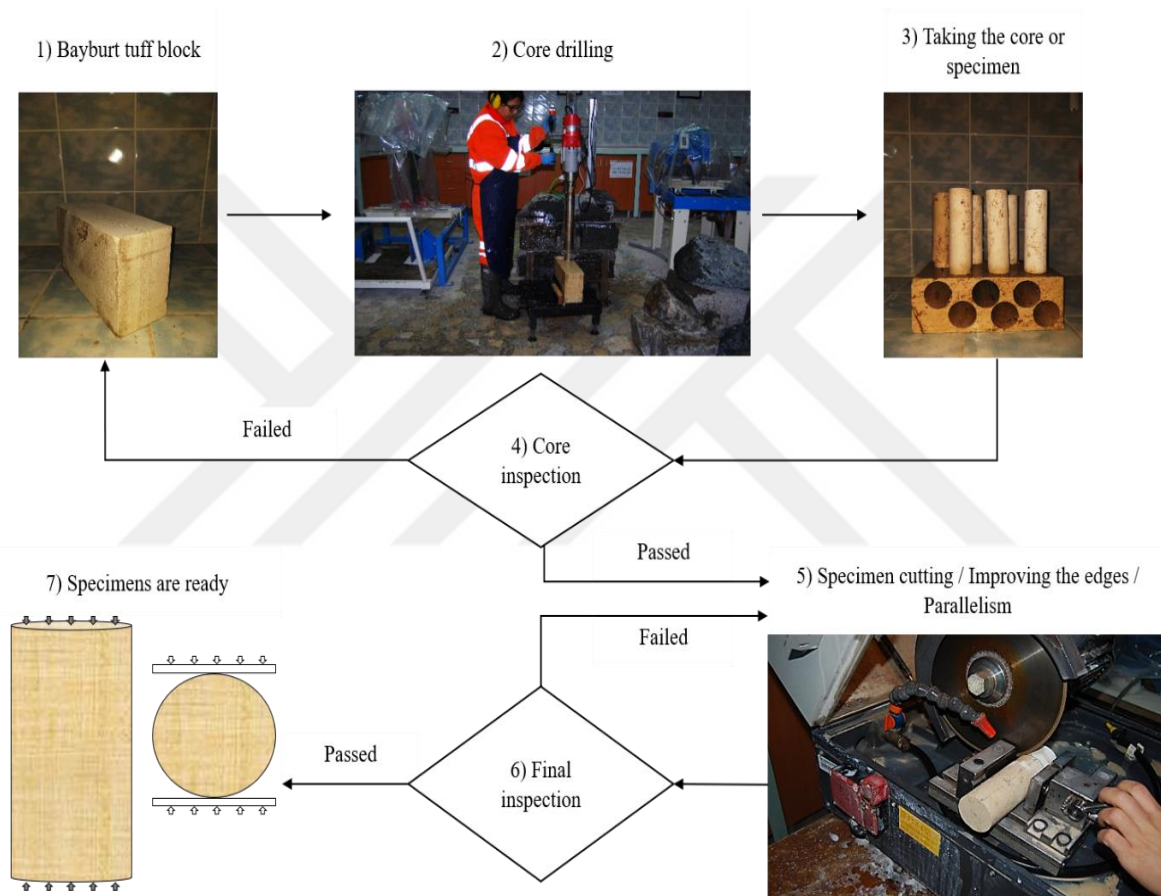


Figure 2.2. Laboratory work flow chart

## 2.2.1. Physico-Mechanical Properties of Bayburt Tuff

### 2.2.1.1. Density Test

Based on the suggestions from ISRM Blue Book (2007) to measure the density of rock specimens, this study applied the following procedure: (a) Five specimens, with a geometry close to a right cylinder, are extracted from a representative intact rock sample. (b) The

measures, both the diameter, height, and weight of specimens, were performed by the Vernier caliper and laboratory balance; however, the average of specimen dimensions will be used for density calculation, see Figure 2.3. (c) The specimen bulk volume is calculated from an average of multiple caliper measures for each dimension. (d) A water immersion saturates the specimens for 48 hours, then the weighing process is repeated for saturated specimens. (e) The specimens are dried to a constant temperature of 105 °C for 48 hours by laboratory drying oven, then the weighing process is repeated for dried specimens.

Assuming as input parameters, the resulting data from the specimen's measurements for the states natural, saturated, and unsaturated. The corresponding densities were calculated and described by Formula 1 and Table 2.1 correspondingly.

$$\text{Density} = \frac{\text{Specimen mass}}{\text{Bulk volume}} \left( \frac{g}{\text{cm}^3} \right) \quad (1)$$

The “specimen mass” depends on the sample's state, which implies that it could be natural, saturated, or unsaturated.



Figure 2.3. Physical measurements from Bayburt tuff specimens

Table 2.1. Densities of Bayburt tuff specimens

Spec	Ht (mm)	Dia (mm)	Bulk Vol (cm <sup>3</sup> )	Specimen Mass			Specimen Density		
				Nat (g)	Unsatd (g)	Satd (g)	Nat (g/cm <sup>3</sup> )	Unsatd (g/cm <sup>3</sup> )	Satd (g/cm <sup>3</sup> )
1	31.42	53.77	71.35	123.10	116.50	133.00	1.73	1.63	1.86
2	31.61	53.80	71.84	123.40	117.00	133.50	1.72	1.63	1.86
3	31.62	53.89	72.13	121.00	114.70	131.60	1.68	1.59	1.82
4	32.33	53.89	73.76	126.40	120.10	136.60	1.71	1.63	1.85
5	32.41	53.86	73.84	126.30	120.10	136.80	1.71	1.63	1.85
Average							1.71	1.62	1.85

The unit weight is calculated by Formula 2.

$$\gamma \text{ (kN/m}^3\text{)} = g \text{ (m/s}^2\text{)} * \rho \text{ (g/cm}^3\text{)} \quad (2)$$

Where “ $\gamma$ ” represents the unit weight of the Bayburt tuff, “ $g$ ” represents the gravity that is  $9.81 \text{ m/s}^2$ , and “ $\rho$ ” represents the rock mass density. Applying this relation, “ $\gamma$ ” was determined as  $16.77 \text{ kN/m}^3$ ,  $15.91 \text{ kN/m}^3$ , and  $18.15 \text{ kN/m}^3$  natural, saturated, and unsaturated, respectively.

#### 2.2.1.2. Determination of Porosity and Void Ratio

In this section, the parameters exhibited in Table 2.1, such as height, diameter, bulk volume, and both natural, saturated, and unsaturated mass, remain as input data to determine the porosity and void ratio using the formulas below.

$$V_v = \frac{M_{sat} - M_{dry}}{\rho_s} \text{ (cm}^3\text{)} \quad (3)$$



$$n = \frac{100 * V_v}{V_s} (\%) \quad (4)$$

$$e = \frac{n}{100 - n} \quad (5)$$

Where “ $V_v$ ” represents the volume of void-space, “ $M_{sat}$ ” represents the specimen’s saturated mass, “ $M_{dry}$ ” represents the specimen’s unsaturated mass, “ $\rho_s$ ” represents the specimen’s density, “ $V_s$ ” represents the volume of the specimen, “ $e$ ” is the void ratio, and “ $n$ ” is the porosity. From Table 2.1, the following input parameters are extracted and Table 2.2 shows the output parameters correspondingly.

$M_{sat}$ : Saturated Mass (g)

$M_{dry}$ : Unsaturated Mass (g)

$\rho_s$ : Natural density (g/cm<sup>3</sup>)

$V_s$ : Bulk volume (cm<sup>3</sup>)

Table 2.2. Volume of void space, porosity, and void ratio of Bayburt tuff specimens

Spec	Volume of void space (cm <sup>3</sup> )	Porosity (%)	Void ratio
1	9.56	13.40	0.15
2	9.61	13.37	0.15
3	10.07	13.97	0.16
4	9.63	13.05	0.15
5	9.76	13.22	0.15
Average	9.73	0.13	0.15

### 2.2.1.3. Uniaxial Compressive Strength Test

Uniaxial compressive strength (UCS) is the single most widely used descriptor of the strength of a particular rock type. UCS test quantifies the peak strength of intact rock, in other words, through of uniaxial compressive stress-strain curve, see Figure 2.4, the specimen will be loaded until its rupture or defeat, exceeding its strength. Nevertheless, not necessarily in this peak strength, the rock can fail because it is not undamaged in earlier

stages below the maximum peak. From Figure 2.4(a), the following stages are identified in Table 2.3.

The output parameter from the UCS test will be the uniaxial compressive strength of the intact rock ( $\sigma_{ci}$ ), defined as the compression strength in which the propagation of fractures in the specimen begins, and its performance depends on control variables, such as loading rate, specimen geometry, specimen size, etc. The specimens were prepared in the Mining Engineering Department's rock mechanics laboratory and performed for UCS test in the Geology Department.

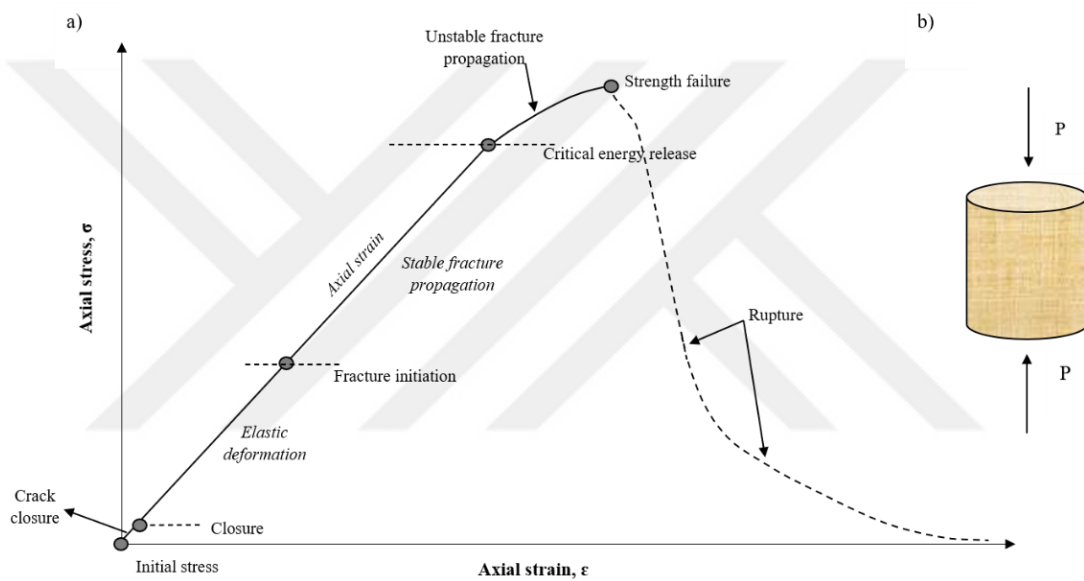


Figure 2.4. Stress-strain curve in geomaterials (H Wang et al., 2010)

Table 2.3. Stages of the stress-strain curve in geomaterials (Wang et al., 2010)

Stage	Name of stage	Description
O-A	Crack closure	Represents that microcrack closure in rocks induces AE signals.
A-B	Elastic deformation	Stage represented by a linear trend where the deformation of mineral crystals from geomaterials supports the external loading.

Continuation of Table 2.3

B-C	Stable fracture propagation	During this stage, the existing microcracks start to extend from their corners. Also, both nonlinear axial and volumetric deformations are measured.
C-D	Unstable fracture propagation	The existing microcracks continuously elongate, and new induced microcracks cause the increasing density of microcracks in geomaterials.
D	Strength failure	The maximum strength failure happens.

Figure 2.5 shows five specimens (with length and diameter of 139.18 mm and 53.98 mm, respectively) subjected to the UCS test to determine the rock's strength against load, and the results show in Table 2.4. In addition to the calculations, the specimen's mode rupture is a criterion to consider the test valid or not, and for this set was the shear failure with conjugates, see Figure 2.6, which means that the UCS tests are proper.

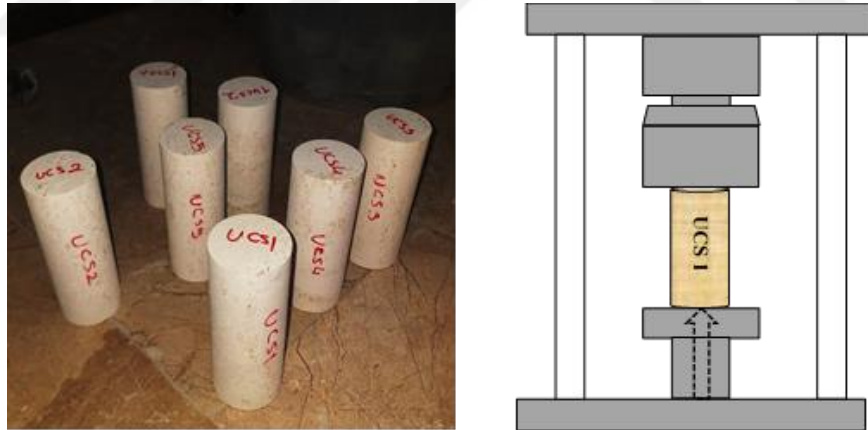


Figure 2.5. UCS test for Bayburt tuff specimens

Table 2.4. UCS test results applied to Bayburt tuff specimens in their natural state

Spec	Length (mm)	Diameter (mm)	Failure Load (kN)	UCS, $\sigma_{ci}$ (MPa)
UCS1	139.99	54.70	99.26	42.24
UCS2	139.66	54.70	100.35	42.70

Continuation of Table 2.4

UCS3	136.95	54.70	93.18	39.65
UCS4	139.07	54.70	104.23	44.35
UCS5	139.64	54.70	83.28	35.44
Average	139.06	54.70	96.06	40.88

Since uniaxial compressive strength average ( $\sigma_{ci\_avg}$ ) was calculated as 40.88 MPa, and based on Table 2.5, Bayburt tuff is a rock of low strength.

Table 2.5. Engineering classification for intact rock (Deere and Miller, 1966)

Class	Description	UCS, $\sigma_{ci}$ , (MPa)
A	Very high strength	Over 220.64
B	High strength	110.32-220.64
C	Medium strength	55.16-110.32
D	Low strength	27.58-55.16
E	Very low strength	Less than 27.58



Figure 2.6. Rock specimens exhibit a shear failure with conjugates

#### 2.2.1.4. Young's Modulus and Poisson's Ratio

The Young's modulus evaluates the relationship between the material deformation and the stress needed to deform it; parameters that are related by Hooke's Law, see Formula 6, where the stress, strain, and young's modulus are represented by  $\sigma$ ,  $\epsilon$ , and  $E$  respectively.

$$\sigma = E * \epsilon \quad (6)$$

The ISRM (2007) develops a methodology to determine the stress-strain curves, Young's modulus, and Poisson's ratio in uniaxial compression for a rock specimen of regular geometry. In the static loads' case, the elasticity test required two Bayburt tuff specimens, where the testing machine subjected each specimen to different ranges of load intensity. The characteristics of cylindrical specimens are an approximate diameter of 54.70 mm, an approximate height of 139.00 mm, and smooth surfaces. Figure 2.7 shows the specimen's arrangement, where "Lo" is the original measured axial length, the compressometer, and two LVDT (linear variable differential transformer) arranged in portrait orientation. Figure 2.8 displays the specimen subjected to the elasticity test by uniaxial compression equipment connected to a computer, where the deformation values due to uniaxial load increases are recorded. This test's output is the stress-strain curve, which defines the axial stress change ratio to axial strain produced by the stress change (ISRM, 2007). The elasticity modulus of Bayburt tuff in the range from 5% to 95%, see Figure 2.9.

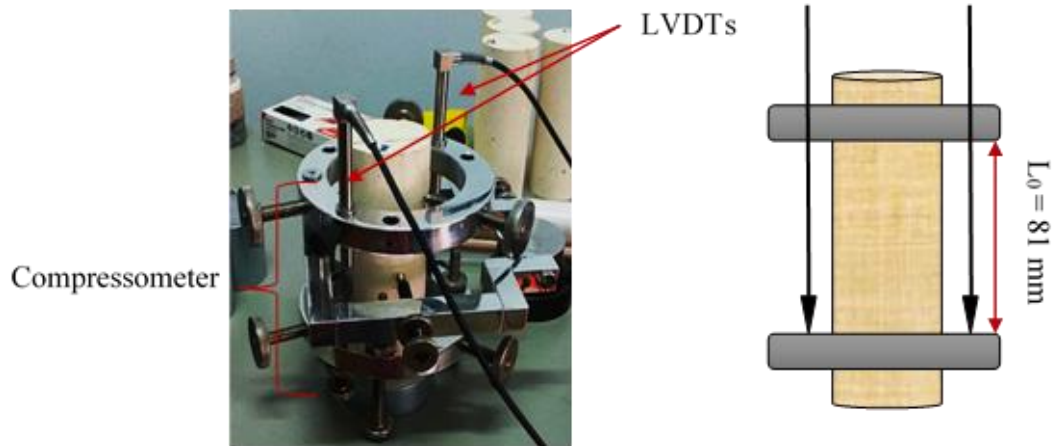


Figure 2.7. Bayburt tuff arrangement for elasticity test

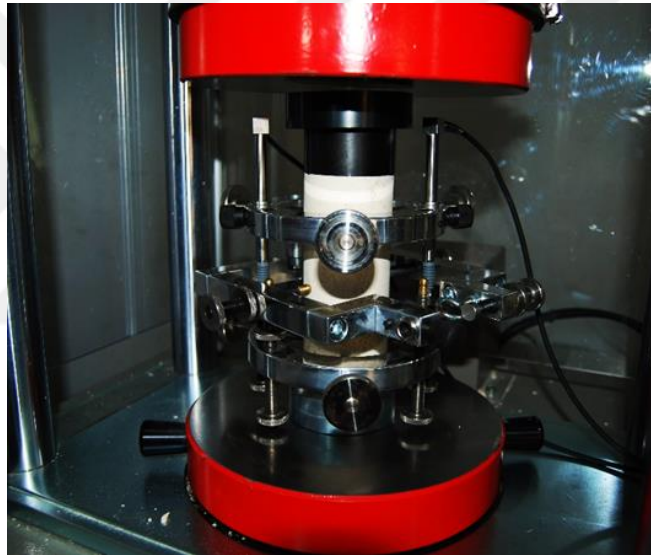


Figure 2.8. Tuff specimen subjected to the elasticity test

The stress-strain curve determines both stresses and vertical strains throughout the whole test; nevertheless, employing the software and devices mentioned in Figure 7 and Figure 8 is achievable to determine the stress that a specimen undergoes and its length variation. Since the software output parameters are the stresses and two extensions (due to two LVDTs), Formula 7 calculates the vertical deformation.

$$\text{Vertical Strain} = \frac{\text{Average of the extensions}}{\text{Original measured axial length}} \quad (7)$$

This study considers an average Young's modulus with a curve range between 5% and 95%, as shown in Table 2.6. On the other hand, Young's modulus for the cyclic loading case will develop in the following sections.

A relevant constant for a given material is its Poisson's ratio. It indicates the relationship between the longitudinal deformations (perpendicular and parallel) and the material applied force. According to Gunderwar (2014), Poisson's ratio for many materials is between 0.15 and 0.36 and is often assumed equal to 0.25; nevertheless, for most rocks, the Poisson coefficient varies between 0.25 and 0.33 (Gonzalez de Vallejo and Ferrer, 2011), but mainly the tuff is in a range of 0.24 - 0.30. Since the Bayburt tuff possesses a low resistance and to be conservative with the FEM simulations, this thesis considers a Poisson's ratio of 0.30.

Table 2.6. Young's modulus for Bayburt tuff for static loading case

Case	Dimension		Young's modulus, E, (MPa)
	Diameter (mm)	Height (mm)	
Static load	53.69	139.07	7581.83

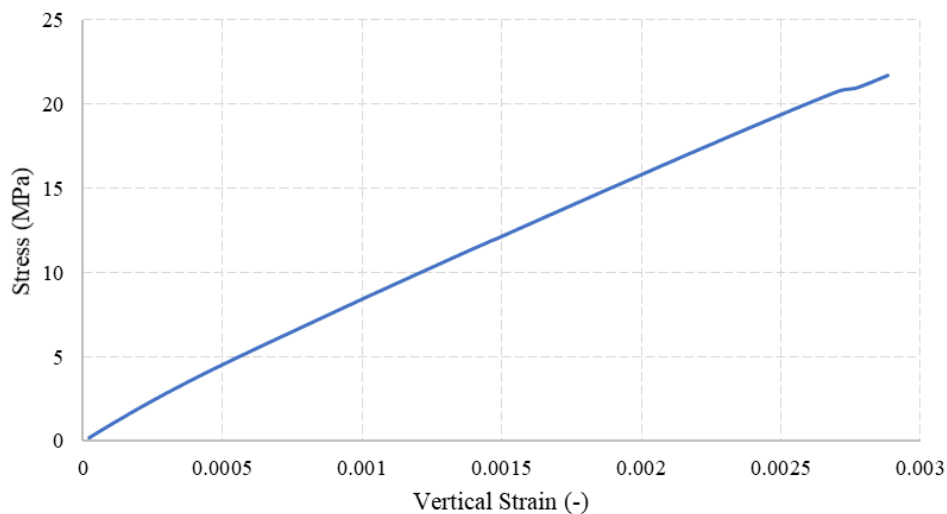


Figure 2.9. Stress-strain curve for static loads case in the range of 5% - 95%

### 2.2.1.5. Brazilian Tensile Strength (BTS) Test

The indirect tensile strength test, see Figure 2.10, consists of diametrically loading a rock disc to determine the tensile strength ( $\sigma_t$ ) that usually develops at the disc's center. In other words, the indirect tensile strength is typically calculated based on the assumption that failure occurs at the point of maximum tensile stress (Li & Wong, 2013), which is located in the center of the disc. Figure 2.11 displays the quantity and geometry of the Bayburt tuff specimens with lengths and diameters of 31.20 mm and 53.77 mm, respectively, as well as a sketch of the BTS test.

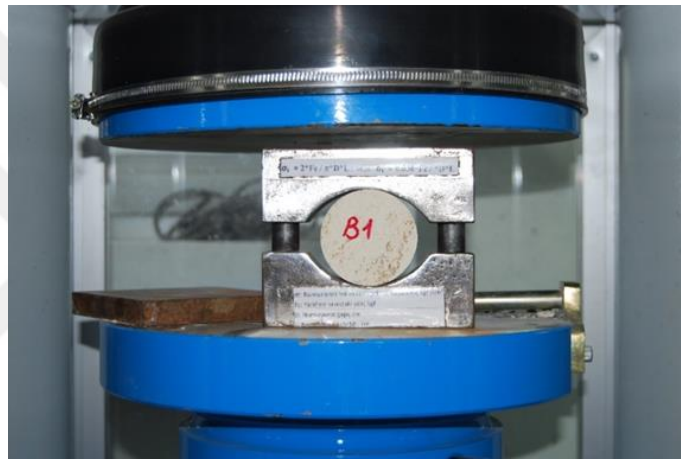


Figure 2.10. Brazilian or indirect tensile strength test

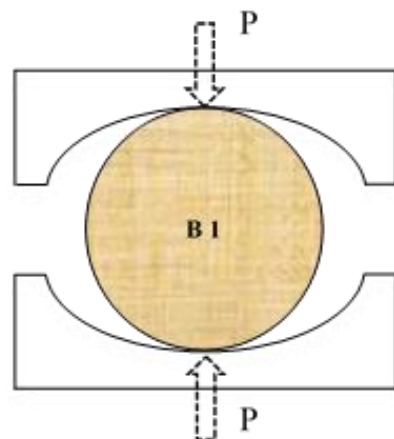


Figure 2.11. BTS test for Bayburt tuff specimens



The failure load ( $P$ ) is recorded, and the tensile strength of the specimen can be calculated using the following Formula 8 proposed by ISMR Blue Book (2007) guidelines for BTS testing.

$$\sigma_t = \frac{2 * P}{\pi * t * D} = 0.636 \frac{P}{D * t} \quad (8)$$

Where “ $\sigma_t$ ” is the tensile strength (MPa), “ $P$ ” is the failure load (N), “ $t$ ” is the thickness of the specimen (mm), and “ $D$ ” the diameter of the specimen (mm).

BTS test were performed according to ISRM (2007) guidelines, as detailed below: (i) the thickness to diameter ratio should be 0.5 to 0.6, and a diameter of approximately 54 mm means a thickness between 27–32.4 mm. (ii) any irregularities across the specimen’s thickness should not exceed 0.025 mm; the end faces shall be flat to within 0.25 mm, square, and parallel to within 0.25°.

The results show in Table 2.7, where the value of “ $P$ ” was estimated, and then apply Formula 8 to obtain “ $\sigma_t$ ”, and  $\sigma_{t\_avg} = 3.95$  MPa was determined. With the BTS test, it must be analyzed the kind of specimen failure to consider this test valid or not; therefore, for the test to be right, the specimen fracture as close as possible to its center. Figure 2.12 shows that the specimens broke in the opening mode, which is when the crack surface displacements are perpendicular to the crack’s plane. (Rossmanith, 1983).

Table 2.7. BTS test results applied to tuff specimens in their natural state

Spec	Thickness (mm)	Diameter (mm)	Failure load (kN)	$\sigma_t$ , (MPa)
B2	31.25	54.00	9.57	3.61
B3	31.46	54.00	10.02	3.76
B4	30.79	54.00	10.11	3.87
B5	31.15	54.00	9.00	3.41
B6	30.85	54.00	10.80	4.13
B7	31.12	54.00	12.34	4.67
B8	31.12	54.00	8.46	3.20

Continuation of Table 2.7

B9	31.26	54.00	10.04	3.79
B10	30.96	54.00	12.56	4.78
Average	31.13	54.00	10.43	3.95

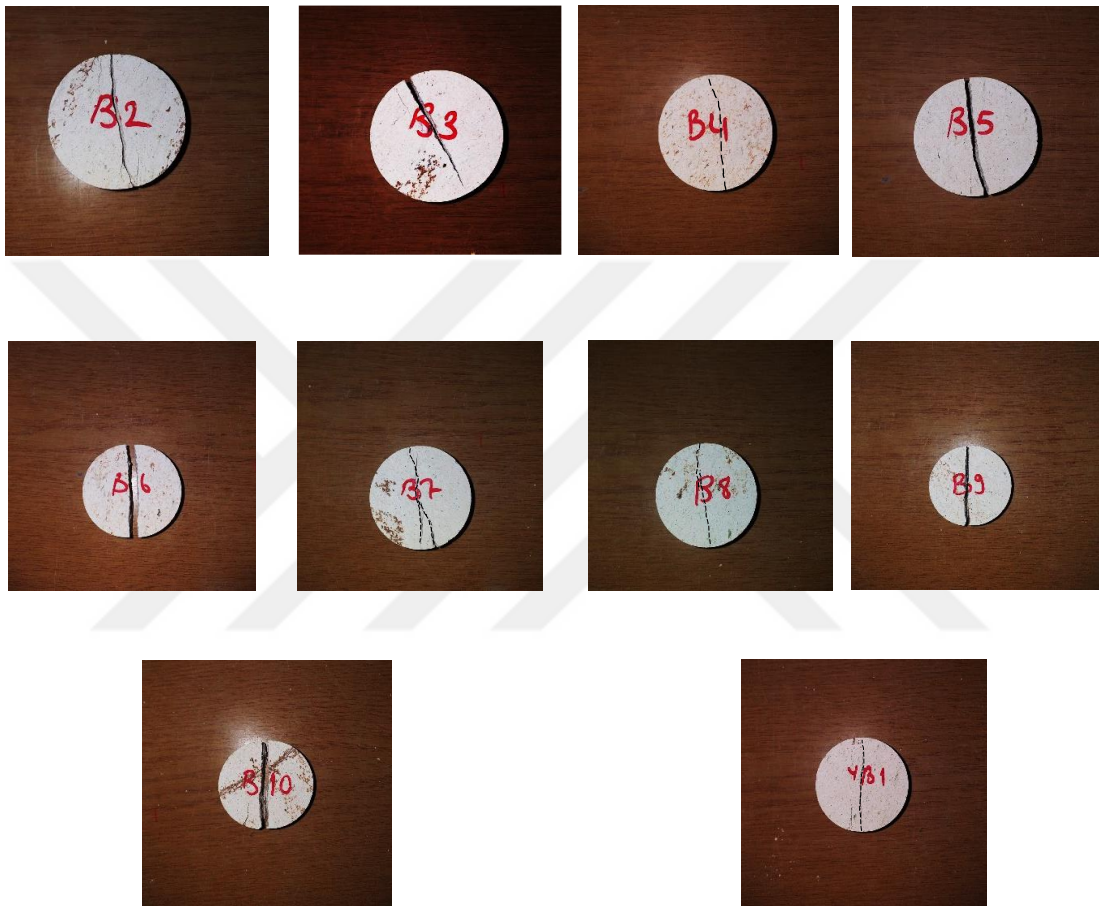


Figure 2.12. Bayburt tuff failure mode after BTS tests

### 2.2.2. Cyclic Loading Test

The preceding sections have described the specimen's rock behaviour when they are subject to continuous stress until their failure through UCS, BTS, and elasticity tests; nevertheless, this behaviour will be different when the specimens are subject to variable loads over time. In this case, rupture can happen at a strength much smaller than the static breaking strength; this phenomenon is known as fatigue.

Fatigue can be defined in the words of ASTM (2000) as follow: “The process of progressive localized permanent structural change occurring in a material subjected to conditions that produce fluctuating stresses and strains at some point or points and that may culminate in cracks or complete fracture after a sufficient number of fluctuations”; moreover, the nature of this phenomenon allows its application in several areas; particularly in the rock fracture mechanics.

“Rock fatigue” is a term used by Singh (1989) to describe rock’s weakening under cyclic loads, where the number of loading cycles to cause a specimen’s failure through repeated and reverse loadings can be determined experimentally for any given maximum and minimum stress level, and frequency. In other words, cyclic loading tests happen in conditions where is determined both minimum and maximum strengths, being the last one lower than static strength failure ( $\sigma_{ci\_avg}$ ). The fatigue test requires input parameters such as predefined loading amplitude and frequency to measure the rock fatigue strength until its defeat for a predetermined number of cycles. For this study, the frequency will be variable; meanwhile, the others will be constant.

Bayburt tuff stress-strain diagram fits the brittle material category, see Figure 2.9. The thesis deduces this statement as a result of comparing three different kinds of stress-strain diagrams shown in Figure 2.13, where (a) and (b) refer to the investigations of Song, Wang & Ren (2019), and Erarslan & Ghamposar (2014) respectively that are curves describe a behaviour typical of brittle materials, and the benchmark is the stress-strain diagram proposed by Beer et al. (2015).

On the one hand, brittle material is which one avoids fracture propagation, and as a result, higher deformation stresses are obtained (Annicchini, 2019); on the other hand, “brittle rock often fails in tension with the inelastic behaviour taking the form of microcracking at the crack tip” Rossmanith (1983). Considering that the fatigue effect is associated with flaws, this refers to the concentration, distribution, and direction in the rock structure; it is necessary to pay attention to the evolution of fractures on the specimen.

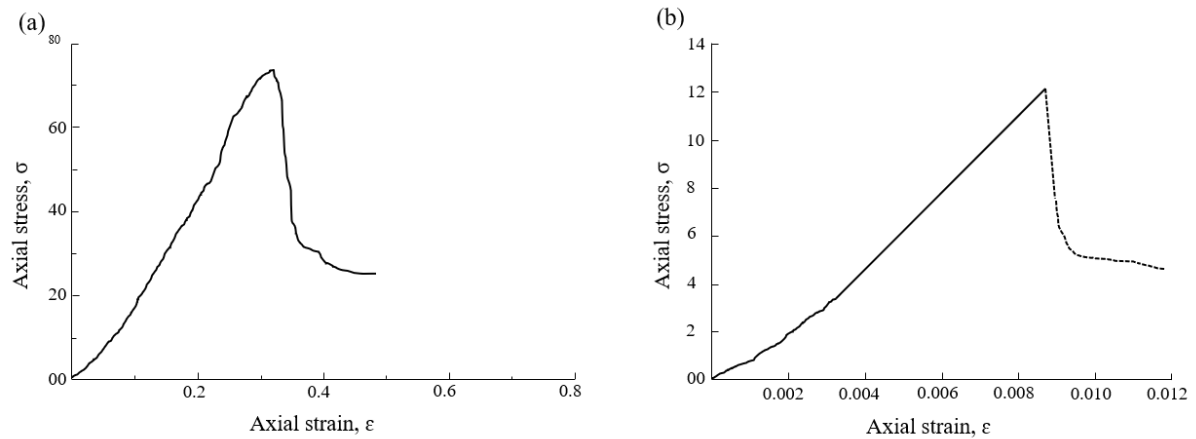


Figure 2.13. Stress-strain curve (a) of Liaoning tuff, and (b) of Brisbane tuff

### 2.2.2.1. Cyclic Loading Test Methodology on Bayburt Tuff

A BESMAK electromechanics test rig is used for cyclic loading and involve the following three steps: (1) The input parameters are defined, where the amplitude and the number of cycles remain constants while performing the test for three types of frequencies. (2) A total of nine cyclic loads tests are performed in three groups, where each set requires a different frequency than the previous one. (3) In each set, after the cyclic loading test, the specimen is subjected to the UCS test to determine the uniaxial compressive strength; besides, the elasticity test is applied to the third sample to estimate Young's modulus. For more details, see Figure 2.14.

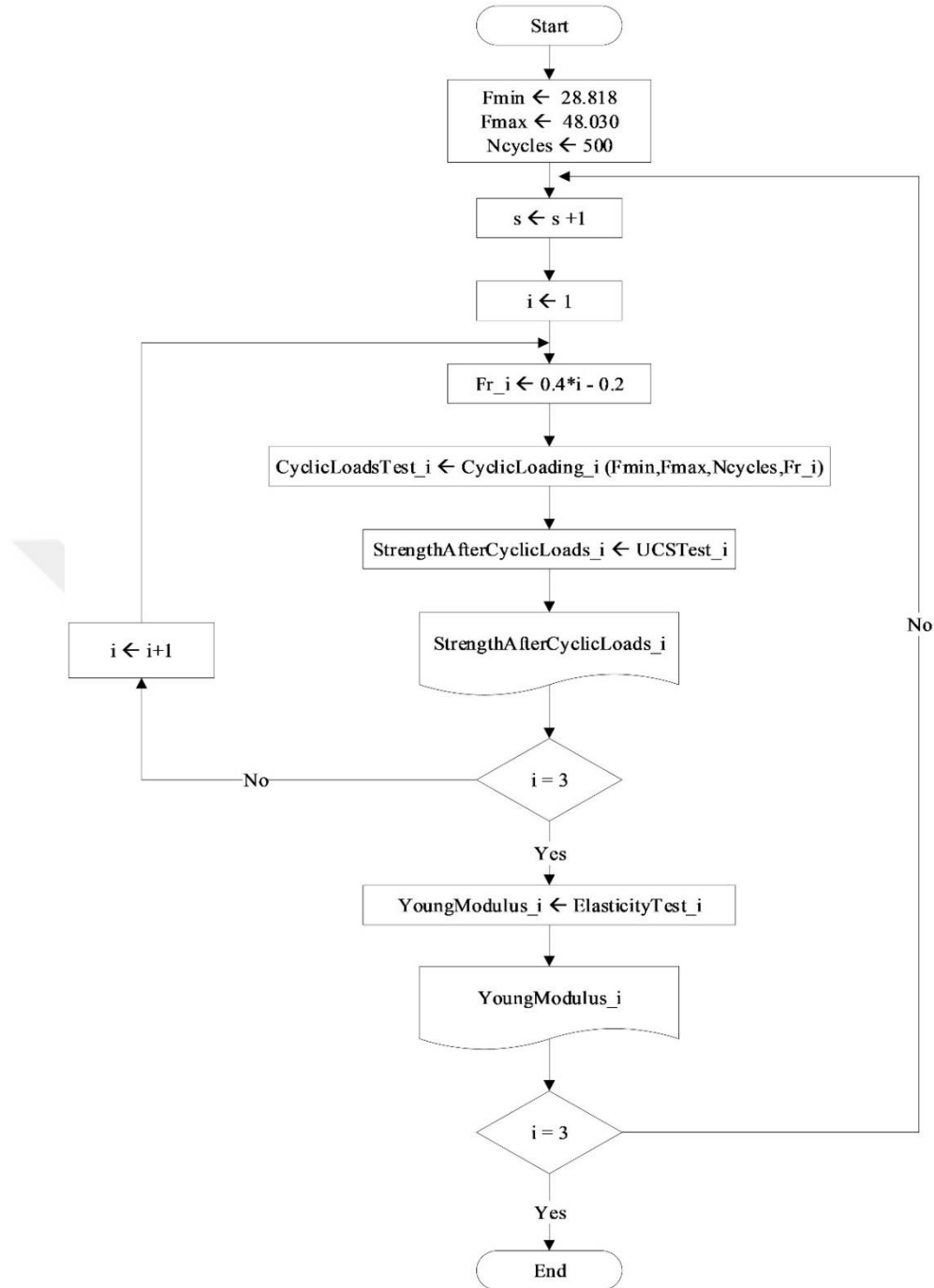


Figure 2.14. Flow chart for the cyclic loading tests

Figure 2.14 describes the modus operandi for the cyclic loading tests, where the following input parameters are defined by Table 2.8. When entering the diagram, it automatically refers to the first set through the “ $s \leftarrow 1$ ” process, where the “ $i \leftarrow 1$ ” action defines the first Bayburt tuff specimen; see Figure 2.15(a). The first loop starts with the first specimen from the first set, where the frequency is calculated by the “ $f_i \leftarrow 0.4*i - 0.2$ ”

process, which for an “i” equal to 1, the frequency, “f\_1”, will be 0.2 Hz; and then conduct the cyclic loading test via “CyclicLoadsTests\_i ← CyclicLoading\_i (Fmin, Fmax, Ncycles, f\_i)” action, see Figure 2.15(b), whose constant factors are “Fmin,” “Fmax,” and “Ncycles,” and the variable to be analyzed is “f.” Figure 2.15(c) refers to the specimen state after the UCS test. The same path will use for an “i” equal to 2 and 3.

Table 2.8. Input parameters for cyclic loading tests

Name of input	Description	Unit
Fmax	It is a constant throughout the cyclic loads' test, indicating the maximum stress level experienced by a Bayburt tuff specimen. This parameter will be equal to 48.030 kN	kN
Fmin	It is a constant throughout the cyclic loads' test, indicating the minimum stress level experienced by a Bayburt tuff specimen. This parameter will be equal to 28.818 kN	kN
Ncycles	It is a constant throughout the cyclic loads' test, alluding to the total number of cycles applied to each Bayburt tuff specimen. This parameter will be equal to 500.	-
F	It is the parameter to be analyzed, referring to the frequency experienced by a Bayburt tuff specimen.	Hz
s	Represents the number of sets or group.	-
i	Refers to the specimen that is being analyzed.	-

Cyclic loading test execution is summed up in a linear variation signal of load wave, as shown in Figure 2.16 for the first specimen from the first set. Afterward, the UCS test performs on the specimen to determine the value of uniaxial strength after cyclic loads' test, see Figure 2.17, a procedure developed and reported by “StrengthAfterCyclicLoads\_i ← UCSTest\_i.” and “StrengthAfterCyclicLoads\_i,” respectively.



Figure 2.15. Bayburt tuff specimen subjected to UCS and cyclic loading test

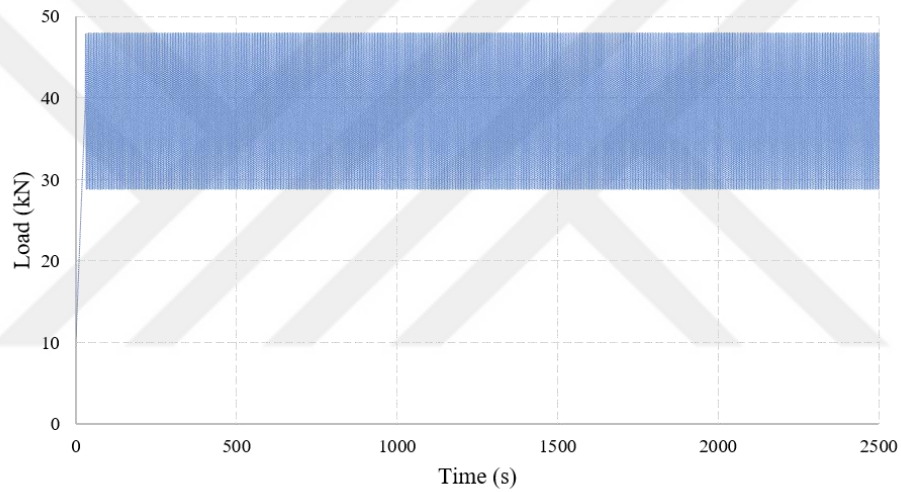


Figure 2.16. Cyclic loading distribution for specimen UF 1-1 (0.2 Hz)

Nevertheless, when “i” is equal to 3, we proceed with the elasticity test to find Young’s Modulus of specimen number 3 from the first set, see Figure 2.18. Finally, the last loop conducts the iterations concerning the working set, “s,” which goes from the first to the third set.

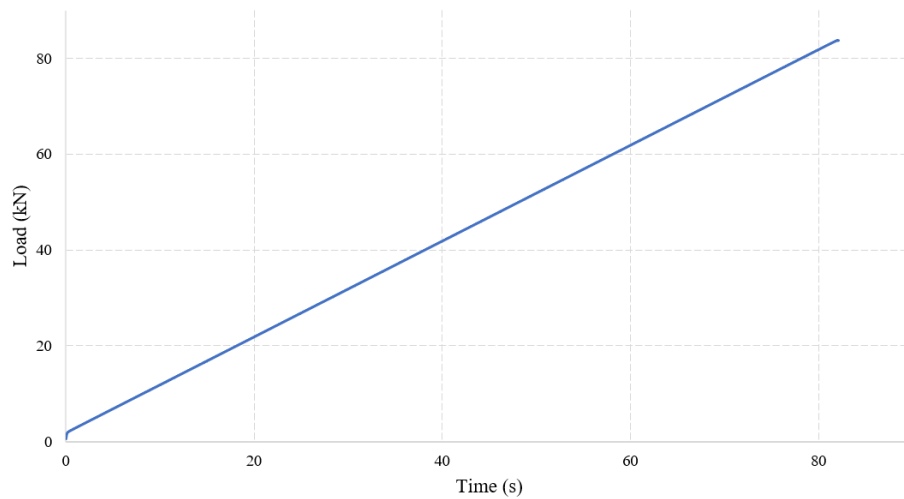


Figure 2.17. UCS curve after cyclic loading test for specimen UF 1-1 (0.2 Hz)

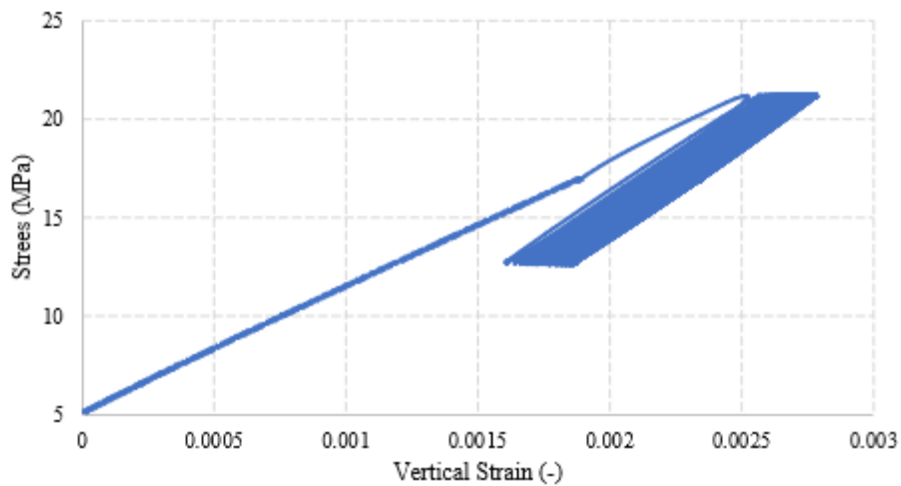


Figure 2.18. Stress-strain curve and cyclic loading test for specimen UF 1-3 (0.2 Hz)

The results of the cyclic loading test are summarized in Table 2.9. Since each sample involves performing both the cyclic load test and the uniaxial compressive strength test; also, the elasticity test applies to every third specimen from each set, which means in 21 curves reported by Annexes.



Table 2.9. Output parameters after cyclic and static loading tests

Set	Spec	Frequency (Hz)	Breaking load (kN)	Uniaxial strength (MPa)	Uniaxial strength average (MPa)	Young' modulus (GPa)
	B-UF1-1		83.814	37.381		
1	B-UF1-2	0.2	98.920	43.568	40.713	5.670
	B-UF1-3		93.407	41.191		
	B-UF2-1		91.361	40.194		
2	B-UF2-2	0.6	98.823	43.482	43.143	6.226
	B-UF2-3		103.779	45.753		
	B-UF3-1		94.572	41.663		
3	B-UF3-2	1.0	96.431	42.467	43.375	6.776
	B-UF3-3		104.390	45.994		

### 3. NUMERICAL SIMULATION BY FEM

#### 3.1. Introduction to Finite Element Method

Based on the fact that understanding and prediction of many physical phenomena involve the use of mathematical models, which implies physical quantities with temporal or spatial variations (Partial Differential Equation or PDE). Unlike algebraic equations, which have numerical quantities as solutions, PDE solutions are functions, which means approximate solutions. Figure 3.1 shows two ways of approaching a physical problem based on its complexity.

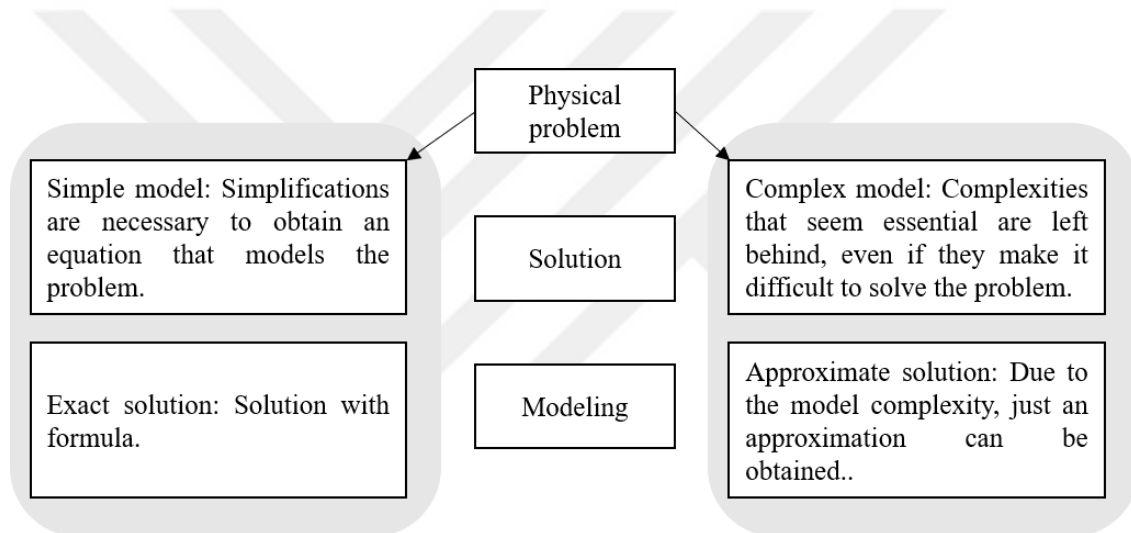


Figure 3.1. Two ways to solve a problem

In engineering structures, it is usual to work with complex models and analyzing through simulation of scenarios. In this context, simulation implies a numerical solution of a complex model to approximate a solution, and the numerical methods appear as a route to obtain approximate solutions for these problems. Inside the numerical methods universe, the following are to be pointed out: finite difference method, finite element method, and boundary element method.

“The finite element method (FEM) is so powerful that many very complicated engineering problems can be solved by it” (Zhu, 2018). FEM is a numerical method that provides an approximate solution to mathematical models, which describe a physical

behaviour in a continuum, typical in engineering. Table 3.1 describes the parameters to take into account to develop in FEM.

Table 3.1. Mandatory parameters in FEM

Parameter	Description
Mathematical model	Refers to differential equations with their boundary conditions.
Physical behaviour	The physical representation of a continuum establishes this behaviour, that is to say, elaborating a physical model of the problem to be analyzed.
Continuum	Real structures under analysis. Model formed by infinite points, where each point has an infinite number of possible displacements or degrees of freedom. In the same way, each point has an infinite number of variables to be determined.

### 3.1.1. Basic Principles of the Finite Element Method

FEM consists of establishing an approximate solution that satisfies a continuum model, see Figure 3.2. FEM obtains a real model's approximate solution, applying a numerical method to a discretized model of a continuum. More specifically, this method finds the discrete model solution from its domain points.

A discretized or simplified model is made up of finite points, where each one from the model possesses a finite number of displacements or degrees of freedom (DOF). Consequently, each point has a finite number of variables to be determined.

The finite elements are connected by interfaces and nodal points; on the other hand, the set of finite elements and nodes is called the finite element mesh. The parts of a discretized models are exposed by Figure 3.3.

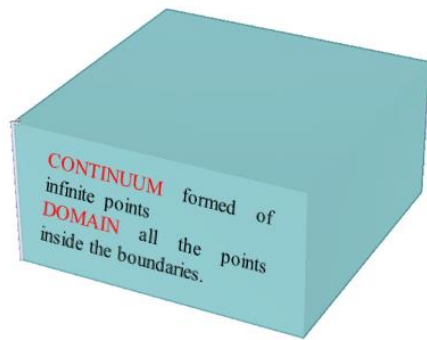


Figure 3.2. Continuum model

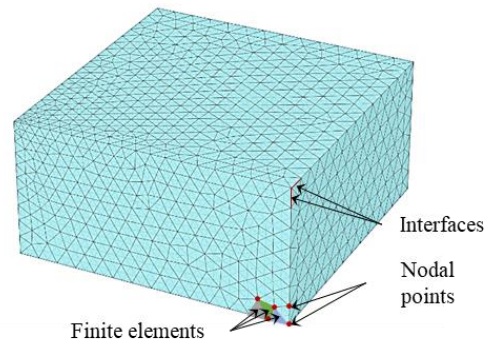


Figure 3.3. Parts of a discretized model

The finite elements can take different shapes, such as triangular, quadrilateral, or cubic. The development of unidimensional, bidimensional, or tridimensional depends on the magnitude of the structure, its analysis, and the commercial software. In this thesis, the structure under study is a hypothetical NATM tunnel developed under Hoek-Brown model to analyze the Bayburt tuff fatigue employing PLAXIS 3D finite element software.

It is logical to say that continuum discretization is a stage; nevertheless, the FEM analysis process consists of a series of stages, as explained in the next section.

#### 3.1.1.1. Analysis Stages By PLAXIS 3D

Alves (2007) reported the majority of FEM commercial software develops three stages to solve a problem: (1) the processing stage, (2) the problem-solving stage, and (3) the post-processing stage or interpretation of results. PLAXIS 3D is a finite element software for the tridimensional analysis of deformation, stability, and ground water flow in geotechnical engineering projects (PLAXIS, 2017). Since this study uses this program for the fatigue analysis and based on PLAXIS 3D Tutorial Manual (2017), which describes four stages for a project, Figure 3.4 shows the stages of solving a problem by PLAXIS 3D finite element software.

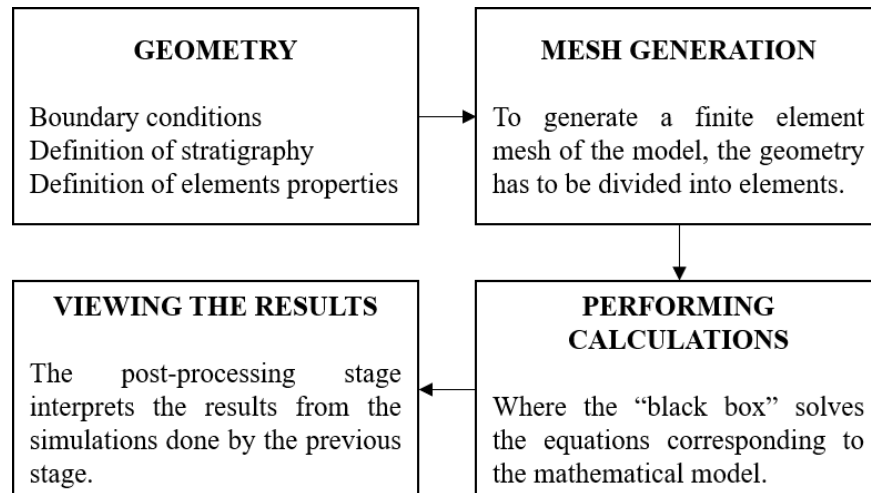


Figure 3.4. Problem analysis stages by PLAXIS 3D Finite Element Software

- i. **Geometry:** On the one hand, this phase consists of a continuum's physic representation; for this purpose, boundary conditions or tridimensional shape of the continuum is established. On the other hand, this stage also defines both the model properties and the structural elements. For instance, the relevant geometry considerations for the research that develops this thesis are the following: (i) The continuum represented for a rectangular parallelepiped shaped. (ii) The Hoek-Brown failure criterion describes the material model. (iii) A hypothetical NATM tunnel is designed as a structural element to be analyzed by PLAXIS 3D finite element software.
- ii. **Mesh generation:** The geometry has to be divided into elements to perform finite element calculations. A composition like this is called a finite element mesh. Meshes in PLAXIS 3D finite element software consists of tetrahedrons with various dimensions that shape the mesh. See Figure 3.5.

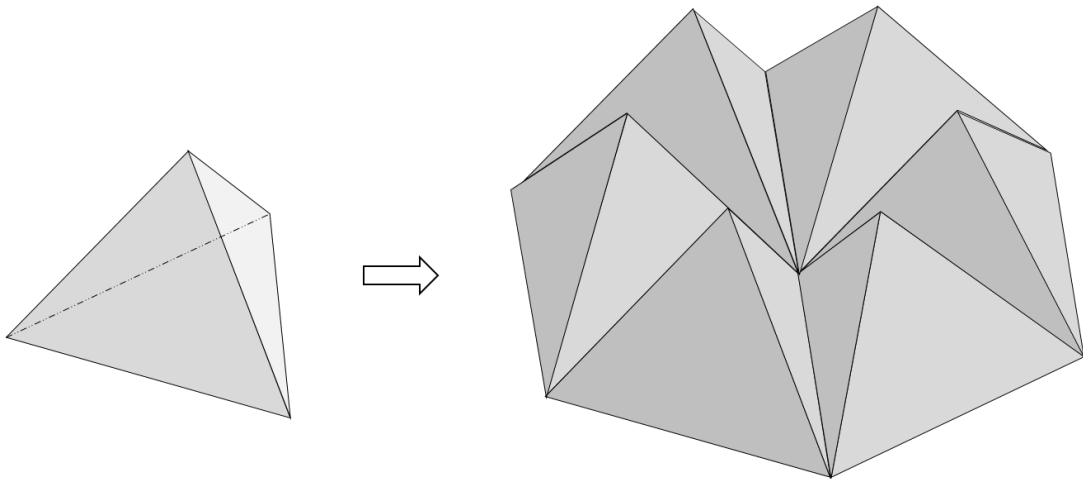


Figure 3.5. The finite element meshing process

- iii. Performing calculations: Stage aiming to numerical calculations of the model through the simulation tool called black box which resolves the mathematical model previously defined, considers its physical principles and assumptions embedded, inputs parameters previously defined in the first stage to figuring out a physical problem's mathematical model. Afterward, a black box obtains a numerical solution, usually a simulation of a scenario, to a particular mathematical model.
- iv. Viewing the results: Once the calculations has been completed, the results are evaluated by this stage.

Figure 3.6 presents the logic process among the four stages mentioned above for a physical problem's numerical solution, resulting in simulation of scenarios. "User inputs" refers to the input parameters defined by Geometry and Mesh generation stages. Performing calculation or Stage III is where PLAXIS 3D finite element software develops and solves the mathematical model, previously defined in Stage I, by the black box. On the one hand, it is solving a mathematical model of the physical problem, and that is based on physical principles assumptions and experimental data. On the other hand, the tool gets selected variables (or target of the project) by evaluating selecting points. Afterward, Stage IV intends to analyze the results.

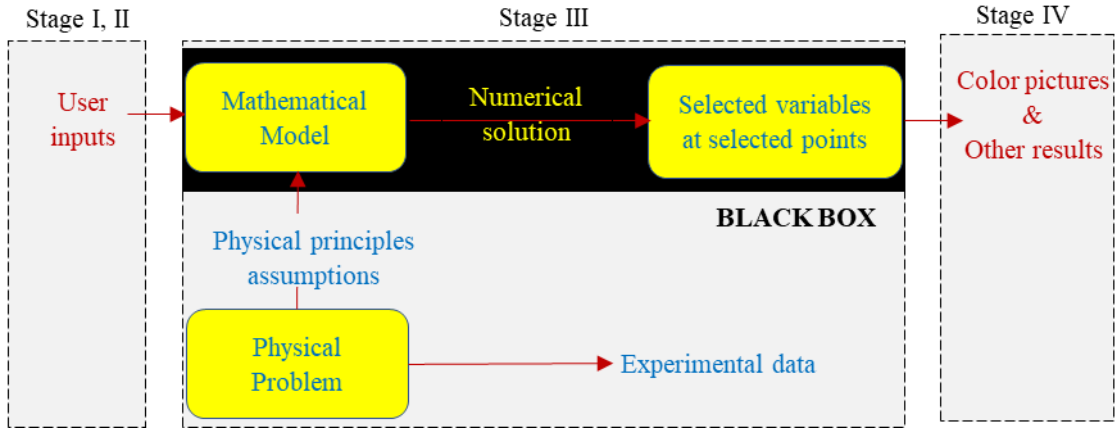


Figure 3.6. Problem solving process by PLAXIS 3D Finite Element Software

### 3.2. Bayburt Tuff Fatigue Analysis Under PLAXIS 3D

It is general knowledge that each engineering project has different conditions and targets. The thesis case focuses on analyzing the Bayburt tuff behaviour for static and cyclic loads scenarios, being the last when the rock mass understudy has been in a state of fatigue. To achieve this purpose, the author performs a hypothetical NATM tunnel design by PLAXIS 3D finite element software for the loads' scenarios mentioned already.

#### 3.2.1. Hoek-Brown Failure Criterion

Hoek-Brown failure criterion is a better non-linear approximation of the strength of rocks, which involves shear strength and tensile strength in a continuous formulation. Hoek (1994) and Hoek et al. (1995) introduced an equation to estimate rock mass strength, known as the generalized Hoek-Brown criterion expressed in Formula 9, representing a non-linear relationship between major and minor effective principal stress, “ $\sigma_1$ ” and “ $\sigma_3$ ”, respectively. Where “ $m_b$ ,” “ $s$ ,” and “ $a$ ” are the rock mass material constants, given by Formula 10, 11, and 12.

$$\sigma_1 = \sigma_3 + \sigma_{ci} \left( m_b \frac{\sigma_3}{\sigma_{ci}} + s \right)^a \quad (9)$$

$$m_b = m_i \exp [(GSI - 100)/(28 - 14D)] \quad (10)$$

$$s = \exp [(GSI - 100)/(9 - 3D)] \quad (11)$$

$$a = 1/2 + 1/6 (e^{-GSI/15} - e^{-20/3}) \quad (12)$$

Applying this criterion to any rock requires considering the formulas already mentioned, but it is also mandatory to define seven key parameters mentioned in Figure 3.7. Since Chapter 2 already defined some parameters, the most relevant ones will be detailed in the following lines.

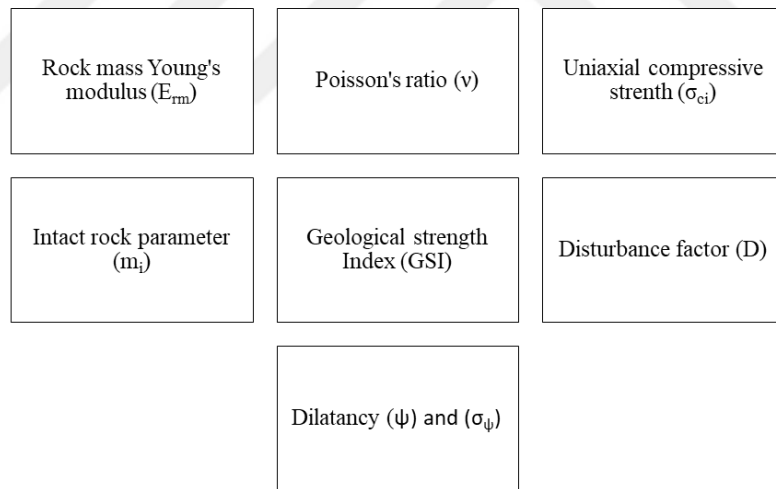


Figure 3.7. Hoek-Brown failure parameters

### 3.2.1.1. The Rock Mass Young's Modulus ( $E_{rm}$ )

The analysis of a tunnel behaviour implies to estimate the deformation modulus of the intact rock mass, " $E_{rm}$ ". To estimate this parameter Plaxis (2017) and Hoek and Brown (2018) advise recommend the Hoek and Diederichs (2016).



$$E_{rm} = E_i \times \left( 0.02 + \frac{1 - D/2}{1 + e^{\left(\frac{60+15D-GSI}{11}\right)}} \right) \quad (13)$$

Where “E<sub>i</sub>” is the intact rock deformation modulus. As can be seen, to use Formula 13, it is necessary to define the values of the Geological Strength Index (GSI) and Disturbance factor (D).

### 3.2.1.2. Intact Rock Parameter (M<sub>i</sub>)

The intact rock parameter (m<sub>i</sub>) is a non-dimensional empirical model parameter that depends on the rock type.

### 3.2.1.3. Dilatancy (Ψ) and Σ<sub>ψ</sub>

The Hoek-Brown model describes the mobilized dilatancy (ψ<sub>mob</sub>) as a function of σ<sub>3</sub> based on two input parameter ψ and σ<sub>ψ</sub>, as can be seen from Formulas 14 and 15.

$$\psi_{mob} = \frac{\sigma_{\psi} + \sigma_3}{\sigma_{\psi}} \times \psi \quad (0 \geq \sigma_3 \geq \sigma_{\psi}) \quad (14)$$

$$\psi_{mob} = \psi + \frac{\sigma_3}{\sigma_t} (90^\circ - \psi) \quad (\sigma_t \geq \sigma_3 \geq \sigma_{\psi}) \quad (15)$$

When the rock is subjected to shear under relatively low confining stress, it shows its dilatant behaviour. This behaviour can be modeled employing a specified value of ψ for σ<sub>3</sub> = 0, which linearly decreases down to zero for σ<sub>3</sub> = σ<sub>ψ</sub>, where σ<sub>ψ</sub> is an additional input parameter.

#### 3.2.1.4. Geological Strength Index (GSI)

The Geological Strength Index (GSI) is an empirical classification system that depends on two factors: the structure or blockiness and the joints' condition. Hoek (1994) and Hoek et al. (1995) introduced it as input data, for rock mass characterization, into numerical analysis or closed solutions for designing tunnels, slopes, or foundations in rock.

In line with GSI's definition formulated by Marinos and Hoek (2000), "From the lithology, structure and surface conditions of the discontinuities, estimate the average value of GSI. Do not try to be too precise. Quoting a range from 33 to 37 is more realistic than  $GSI = 35$ ." However, establishing this parameter is not easy and not exact (P. Ván and B. Vásárhelyi, 2013).

PLAXIS 3D software makes uses of the basic version of the GSI chart from Hoek and Marinos (2000), see Figure 3.8.










GEOLOGICAL STRENGTH INDEX FOR JOINTED ROCKS (Hoek and Marinos, 2000)		SURFACE CONDITIONS				
<p>From the lithology, structure and surface conditions of the discontinuities, estimate the average value of GSI. Do not try to be too precise. Quoting a range from 33 to 37 is more realistic than stating that GSI = 35. Note that the table does not apply to structurally controlled failures. Where weak planar structural planes are present in an unfavourable orientation with respect to the excavation face, these will dominate the rock mass behaviour. The shear strength of surfaces in rocks that are prone to deterioration as a result of changes in moisture content will be reduced if water is present. When working with rocks in the fair to very poor categories, a shift to the right may be made for wet conditions. Water pressure is dealt with by effective stress analysis.</p>		SURFACE CONDITIONS				
		VERY GOOD	GOOD	FAIR	POOR	VERY POOR
STRUCTURE		DECREASING SURFACE QUALITY →				
 <p>INTACT OR MASSIVE - intact rock specimens or massive in situ rock with few widely spaced discontinuities</p>	90			N/A	N/A	
 <p>BLOCKY - well interlocked undisturbed rock mass consisting of cubical blocks formed by three intersecting discontinuity sets</p>	80	70				
 <p>VERY BLOCKY- interlocked, partially disturbed mass with multi-faceted angular blocks formed by 4 or more joint sets</p>		60				
 <p>BLOCKY/DISTURBED/SEAMY - folded with angular blocks formed by many intersecting discontinuity sets. Persistence of bedding planes or schistosity</p>			50	40		
 <p>DISINTEGRATED - poorly interlocked, heavily broken rock mass with mixture of angular and rounded rock pieces</p>				30	20	
 <p>LAMINATED/SHEARED - Lack of blockiness due to close spacing of weak schistosity or shear planes</p>	N/A	N/A			10	

Figure 3.8. Basic GSI chart (Hoek and Marinos, 2000)

**3.2.1.5. Disturbance Factor (D)**

Disturbance factor (D), which depends on the degree of disturbance of the rock-mass produced by the excavation processes., varies from 0 for undisturbed in situ rock masses, to 1, for very disturbed rock masses. Table 3.2 is a guideline that explains the way to estimate D.

Table 3.2. Guidelines for estimating disturbance factor (D)

Appearance of rock mass	Description of rock mass	Suggested value of D
	<p>Excellent quality-controlled blasting or excavation by Tunnel Boring Machine results in minimal disturbance to the confined</p>	D = 0
	<p>Mechanical or hand excavation in poor quality rock masses (no blasting) results in minimal disturbance to the surrounding rock mass.</p> <p>Where squeezing problems results in significant floor heave, disturbance can be severe unless a temporary invert, as shown in the photograph, is placed.</p>	D = 0 D = 0.5 No invert
	<p>Very poor-quality blasting in a hard rock tunnel results in severe local damage, extending 2 or 3 m, in the surrounding rock mass.</p>	D = 0.8

Continuation of Table 3.2



Small scale blasting in civil engineering slopes results in modest rock mass damage, particularly if controlled blasting is used as shown on the left-hand side of the photograph. However, stress relief results in some disturbance.

$D = 0.7$

Good blasting

$D = 1.0$

Poor blasting



Very large open pit mine slopes suffer significant disturbance due to heavy production blasting and also due to stress relief from overburden removal.

$D = 1.0$

Production blasting

$D = 0.7$

In some softer rock excavations can be carried out by ripping and dozing and the degree of damage to the slope is less.

Mechanical  
excavation

### 3.2.2. Excavation of a Hypothetical NATM Tunnel

The New Australian Tunneling (NATM) method is an empirical technique in which rock exposed by excavation is stabilized with rock shotcrete to form a temporary lining. This section illustrates the PLAXIS 3D finite element software use to analyze a hypothetical NATM tunnel construction for static and cyclic loads. On the one hand, this construction involves both the deconfinement method and gravity loading to generate initial stresses. On the other hand, part of the design simulates the Bayburt tuff behaviour for different scenarios under the Hoek-Brown failure criterion.

As suggested before, to simulate through PLAXIS 3D finite element software, four stages are necessary (geometry, mesh generation, performing calculations, and viewing the results). The following pages from these sections provide an organized and logical explanation of the input parameters, assumptions, and simulated scenarios.

### 3.2.3. Stage 1: Geometry

#### 3.2.3.1.1. Definition of Boundary Conditions and Material Properties

The limits of the Bayburt tuff block were defined for the rock contour as  $X_{\min} = -43.00$  m,  $X_{\max} = 57.00$  m,  $Y_{\min} = 0.00$  m, and  $Y_{\max} = 35.00$  m. Moreover, three boreholes define the geometry on the z-axis as  $Z_{\min} = -15.00$  m,  $Z_{\max} = 35.00$  m, which shape an irregular block, as shown in Figure 3.9.

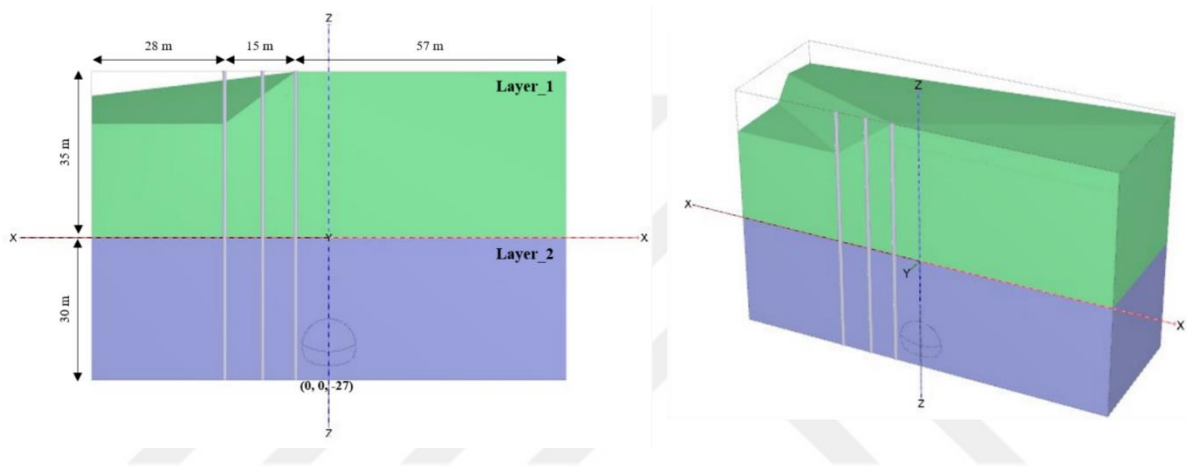


Figure 3.9. Front and three-dimensional view of Bayburt tuff block

Afterward, having defined the tridimensional rock block, this study uses both the laboratory results described in Chapter 2 and the generalized Hoek-Brown failure criterion, already described, to simulate the Bayburt tuff behaviour for static and cyclic load scenarios. The criterion choice is based on its wide range of engineering applications and its optimal application for brittle materials.

Table 3.3 organizes the input parameters requested by PLAXIS 3D finite element software taking into account the Hoek-Brown failure criterion as a model to simulate scenarios already mentioned. At the same time, this table makes mention from where each parameter is extracted and the case of the assumed parameters, each one has been appropriately justified.

Table 3.3. Input parameters requested by PLAXIS 3D Finite Element Software

Parameter	Symbol	Source
Dried density	$\gamma_{\text{unsat}}$	Average extracted from Table 2.1.
Saturated density	$\gamma_{\text{sat}}$	Average extracted from Table 2.1.
Void ratio	$e_{\text{init}}$	Average extracted from Table 2.2.
Young' modulus of the intact rock mass	$E_{\text{rm}}$	“ $E_i$ ” is taken from Table 2.6 (static case) and Table 2.9 (cyclic case). Each value of “ $E_i$ ” is replaced in Formula 13 to obtain “ $E_{\text{rm}}$ .”
Poisson's ratio	$\nu$ (nu)	For rocks, the Poisson coefficient varies between 0.25 and 0.33 (Gonzalez de Vallejo and Ferrer, 2011). This thesis considers a Poisson's ratio of 0.30.
Uniaxial compressive strength	$\sigma_{\text{ci}}$	For static case, “ $\sigma_{\text{ci}}$ ” average extracted from Table 2.4. For cyclic case, “ $\sigma_{\text{ci}}$ ” average extracted from Table 2.9.
Intact rock parameter	$m_i$	This study assumes “ $m_i$ ” as eight, value taken from Plaxis Material Models Manual (2017).
Geological strength index	GSI	For finding the Bayburt tuffs' GSI, this thesis considers a range between 60 and 50 as the GSI value. However, establishing this parameter is not easy and not exact (P. Ván and B. Vásárhelyi, 2013).
Disturbance factor	D	This research assumes a Layer_1 with $D = 0$ , and Layer_2 with $D = 0.5$ . Table 3.2 for more info.
Dilatancy parameter	$\psi_{\text{max}}$	For the finite element simulations, this investigation will use the tuff behaviour values, described Leiva (2013), assuming $\psi_{\text{mob}} = 89.9^\circ$ and $\sigma_\psi = 100$ for layer_1, and $\psi_{\text{mob}} = 30^\circ$ and $\sigma_\psi = 400$ for layer_2.
Dilatancy parameter	$\sigma_\psi$	

Given the experimental part did not have the following two tests: Triaxial Shear Test to obtain the principal stresses ( $\sigma_1$  and  $\sigma_3$ ) for the specimen or Direct Shear Test to determine

residual shear strength, maximum shear strength, friction angles, dilatation angles, as well as the variation of the friction angle with deformation. This study justified these assumptions, the two last parameters mentioned in Table 3.3, based on the Leiva thesis (2013), which reported experimental study results in zeolite tuffs present in Quinamavida, the pre-Andean sector of the Maule Region in Chile.

Having explained, roughly, how PLAXIS works with the Hoek-Brown failure criterion and what are the input parameters for modelling through it. Then, the inputs for the modelling cases for both static loads and cyclic loads are presented by Table 3.4, Table 3.5, Table 3.6, and Table 3.7.

Table 3.4. Material properties of the Bayburt tuff (static case)

Parameter name	Layer_1	Layer_2	Unit
Model	Hoek-Brown	Hoek-Brown	-
Type	Drained	Drained	-
$\gamma_{\text{unsat}}$	15.91	15.91	kN/m <sup>3</sup>
$\gamma_{\text{sat}}$	18.15	18.15	kN/m <sup>3</sup>
$e_{\text{init}}$	0.15	0.15	-
$E_{\text{rm}}$	$4.79 \cdot 10^6$	$2.67 \cdot 10^6$	kN/m <sup>2</sup>
$\nu$	0.30	0.30	-
$\sigma_{\text{ci}}$	$42.33 \cdot 10^3$	$42.33 \cdot 10^3$	kN/m <sup>2</sup>
$m_i$	8	8	-
GSI	55	55	-
D	0	0.5	-
$\Psi_{\text{max}}$	89.9	30	-
$\sigma_{\psi}$	1000	400	kN/m <sup>2</sup>

Table 3.5. Material properties of the Bayburt tuff (cyclic case, 0.2 Hz)

Parameter name	Layer_1	Layer_2	Unit
Model	Hoek-Brown	Hoek-Brown	-
Type	Drained	Drained	-
$\gamma_{\text{unsat}}$	15.91	15.91	kN/m <sup>3</sup>
$\gamma_{\text{sat}}$	18.15	18.15	kN/m <sup>3</sup>
$e_{\text{init}}$	0.15	0.15	-



Continuation of Table 3.5

$E_{rm}$	$3.58 \cdot 10^6$	$2.00 \cdot 10^6$	kN/m <sup>2</sup>
$\nu'$ (nu)	0.30	0.30	-
$\sigma_{ci}$	$40.71 \cdot 10^3$	$40.71 \cdot 10^3$	kN/m <sup>2</sup>
$m_i$	8	8	-
GSI	55	55	-
D	0	0.5	-
$\Psi_{max}$	89.9	30	-
$\sigma_{\psi}$	1000	400	kN/m <sup>2</sup>

Table 3.6. Material properties of the Bayburt tuff (cyclic case, 0.6 Hz)

Parameter name	Layer_1	Layer_2	Unit
Model	Hoek-Brown	Hoek-Brown	-
Type	Drained	Drained	-
$\gamma_{unsat}$	15.91	15.91	kN/m <sup>3</sup>
$\gamma_{sat}$	18.15	18.15	kN/m <sup>3</sup>
$e_{init}$	0.5	0.5	-
$E_{rm}$	$3.93 \cdot 10^6$	$2.20 \cdot 10^6$	kN/m <sup>2</sup>
$\nu'$ (nu)	0.30	0.30	-
$\sigma_{ci}$	$43.14 \cdot 10^3$	$43.14 \cdot 10^3$	kN/m <sup>2</sup>
$m_i$	8	8	-
GSI	55	55	-
D			-
$\Psi_{max}$	89.9	30	-
$\sigma_{\psi}$	1000	400	kN/m <sup>2</sup>

Table 3.7. Material properties of the Bayburt tuff (cyclic case, 1.0 Hz)

Parameter name	Layer_1	Layer_2	Unit
Model	Hoek-Brown	Hoek-Brown	-
Type	Drained	Drained	-
$\gamma_{unsat}$	15.91	15.91	kN/m <sup>3</sup>
$\gamma_{sat}$	18.15	18.15	kN/m <sup>3</sup>
$e_{init}$	0.5	0.5	-

Continuation of Table 3.7

$E_{rm}$	$4.28 \cdot 10^6$	$2.39 \cdot 10^6$	kN/m <sup>2</sup>
$\nu$	0.30	0.30	-
$\sigma_{ci}$	$43.36 \cdot 10^3$	$43.36 \cdot 10^3$	kN/m <sup>2</sup>
$m_i$	8	8	-
GSI	55	55	-
D			-
$\Psi_{max}$	89.9	89.9	-
$\sigma_{\psi}$	0	0	kN/m <sup>2</sup>

### 3.2.3.1.2. Definition of NATM Tunnel Profile

Tunneling involves a significant number of activities that depend on the tunnel profile and its excavation sequence. Since one of the thesis specific objectives aims to carry out a simulation exercise, both the NATM tunnel profile and its sequence were performed, adapting from the Plaxis 2D Tutorial Manual (2018). Figure 3.10 displays this profile.

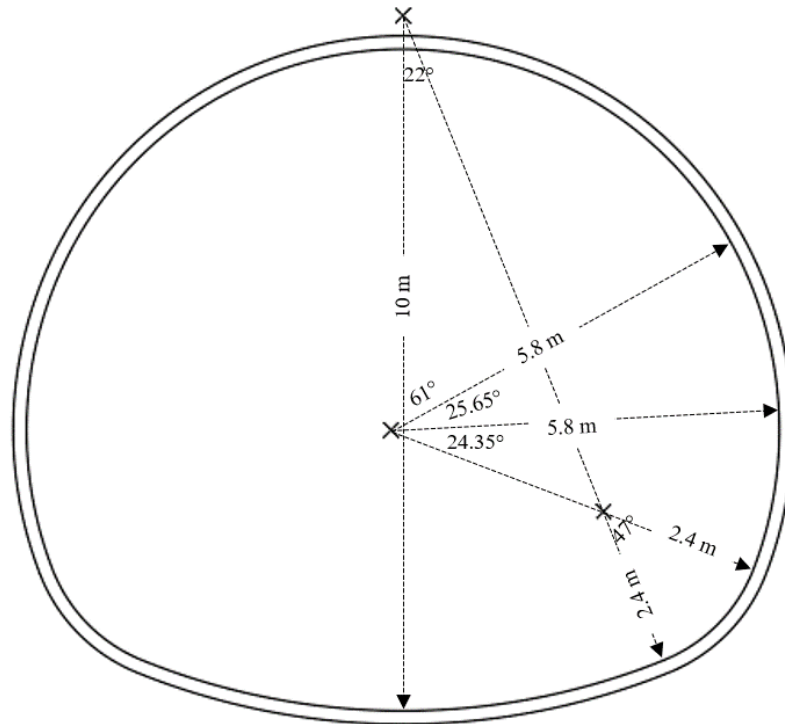


Figure 3.10. NATM tunnel profile, adapted from Plaxis (2018)

The following phases will describe tunnel procedure construction: (1) Phase 1 consists of excavating three linear meters the upper section of the tunnel, as shown Figure 3.11. (b). (2) As a result of the excavation, compression stresses appear in this area, for this reason, phase 2, see Figure 3.11. (c), In theory this phase describes the use of shotcrete as tool support; however, since this study simulates a small part of a hypothetical NATM tunnel, it is agreed not to use shotcrete. (3) In Phase 3, the remaining rock material is extracted; this is the lower section, as shown in Figure 3.11. (d). (4) Phase 4 is responsible for supporting the entire structure, see Figure 3.11. (e).

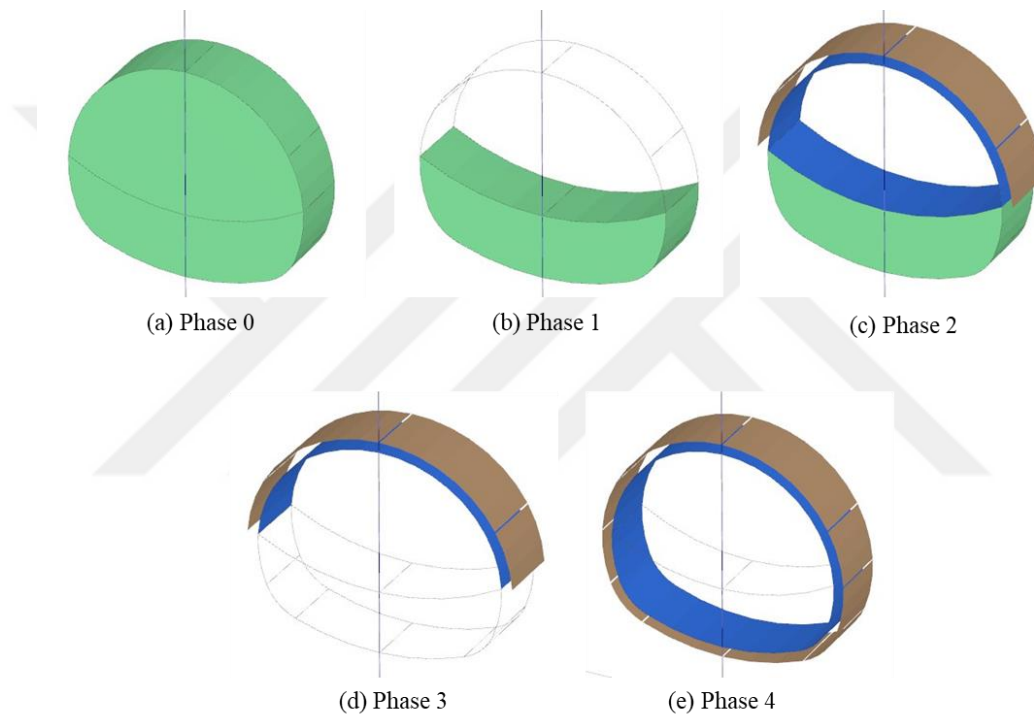


Figure 3.11. Three-dimensional NATM tunnel sequencing phase by phase

### 3.2.3.2. Stage 2: Mesh Generation

The meshing process or discretization allows dividing the model into small finite elements interconnected by nodes, as shown in Figure 3.12.

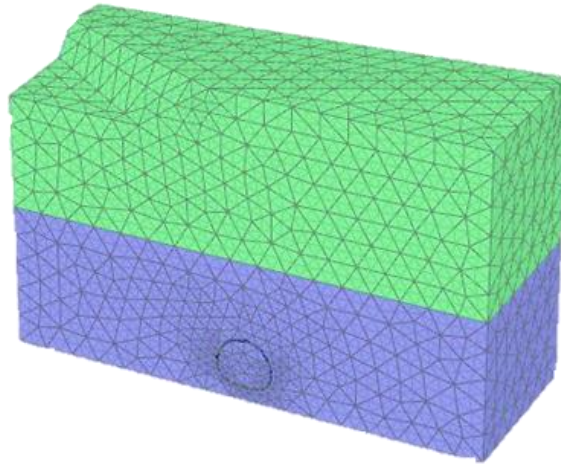


Figure 3.12. Generated mesh for Bayburt tuff block

### 3.2.3.3. Stage 3 and 4: Performing Calculations and Viewing the Results

As explained earlier, the black box is responsible for giving approximate solutions through simulations to mathematical models that define the problem. For this study, a set of mathematical equations describes the Hoek-Brown material model that exposes a relationship between the major and minor effective principal stresses, where infinitesimal increments of stress are related to infinitesimal increments of strain.

Analyzing the fatigue influence in the Bayburt tuff involves comparing both static and cyclic loads. Considering frequency variations (0.2 Hz, 0.6 Hz, and 1.0 Hz) for the dynamic scenarios. The output parameters to evaluate and compare are: total displacements ( $|u|$ ) for each phase, principal total stresses ( $\sigma_3$ ) for each phase, and safety factors (SF) for the tunnel. For more details see Figure 3.13, Figure 3.14, Figure 3.15, Figure 3.16, Figure 3.17, Figure 3.18, Figure 3.19, Figure 3.20, and Figure 3.21.

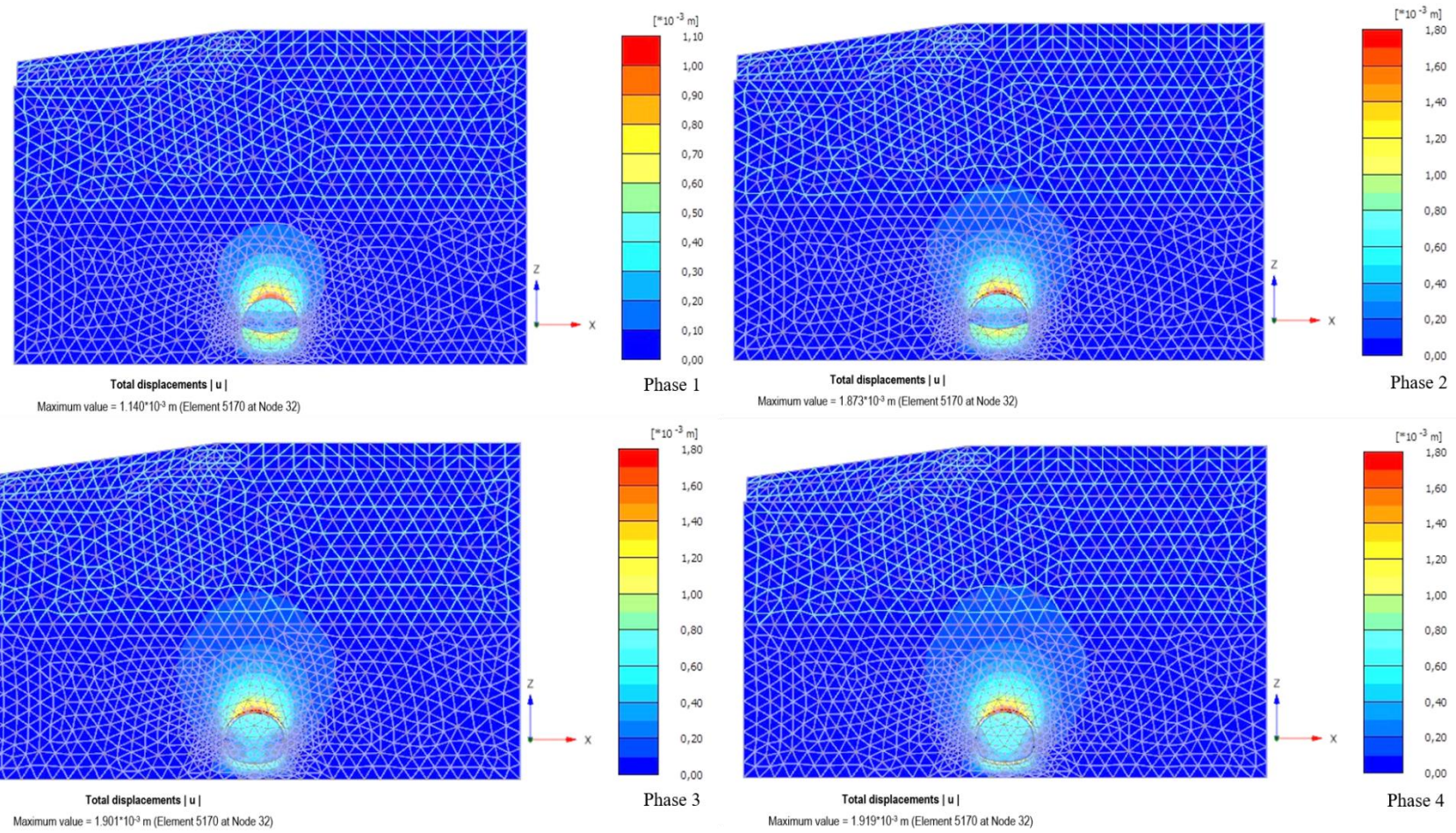


Figure 3.13. Total displacements by phase for static loading case

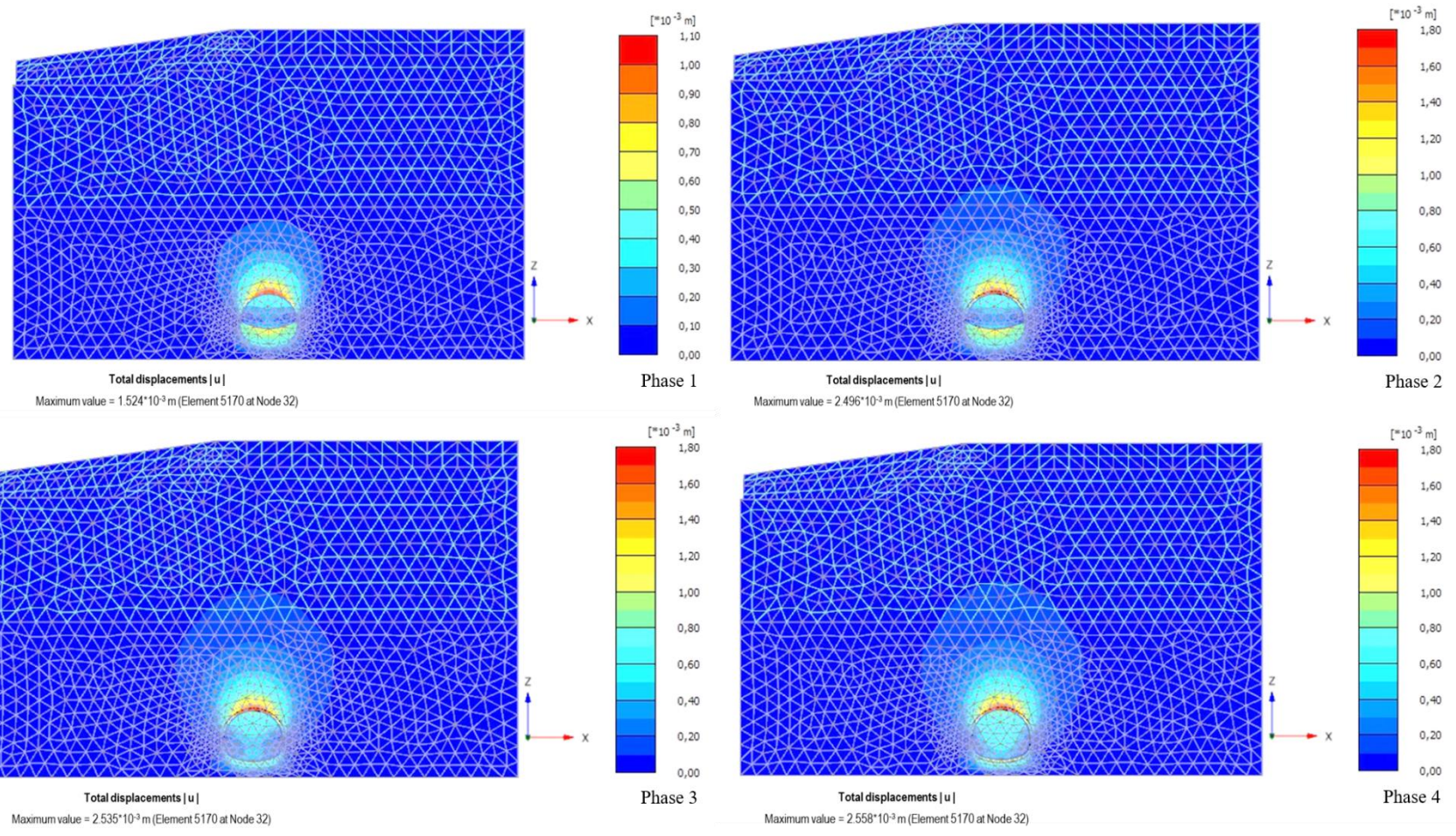


Figure 3.14. Total displacements by phase for cyclic loading case (0.2 Hz)

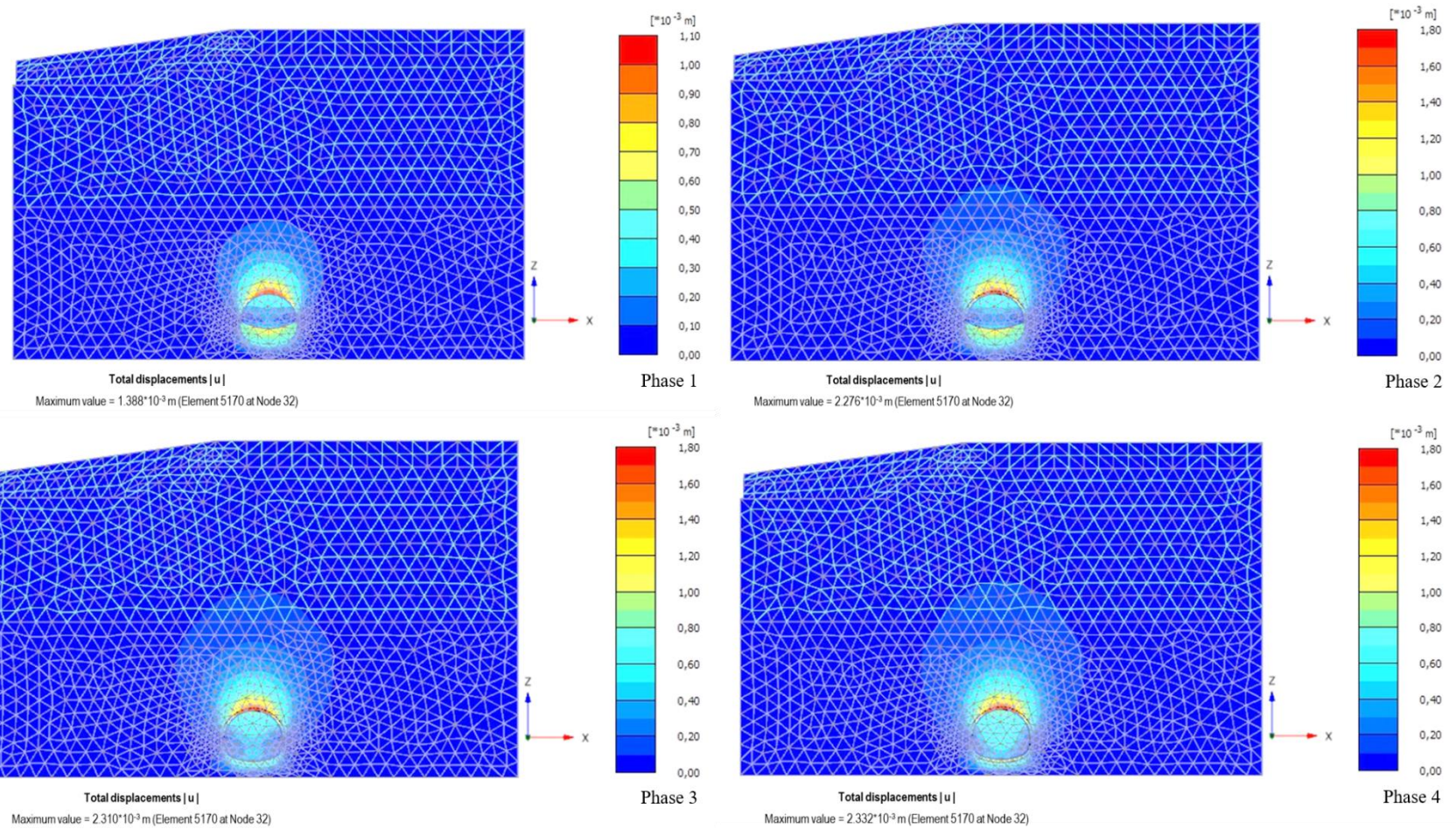


Figure 3.15. Total displacements by phase for cyclic loading case (0.6 Hz)

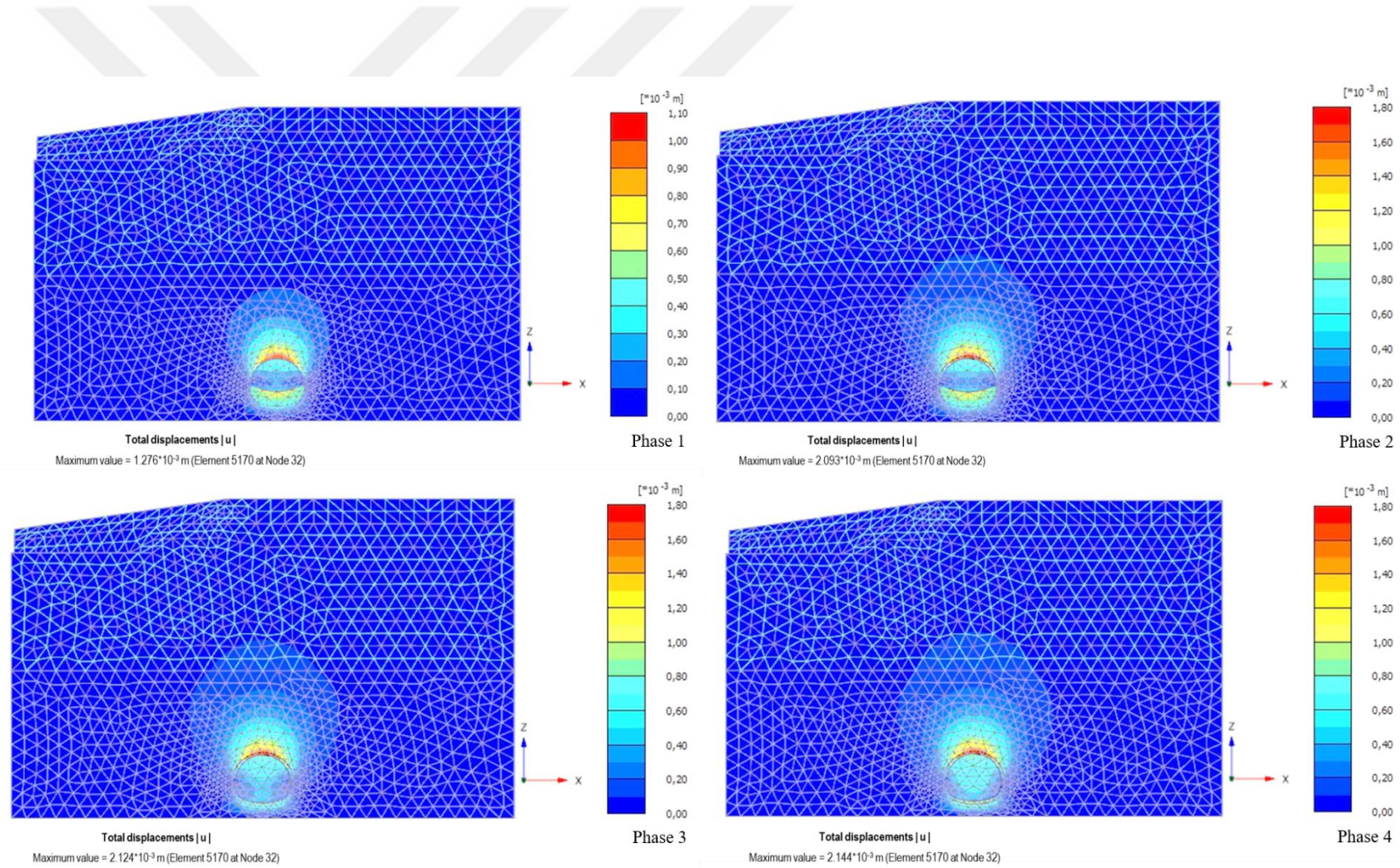


Figure 3.16. Total displacements by phase for cyclic loading case (1.0 Hz)



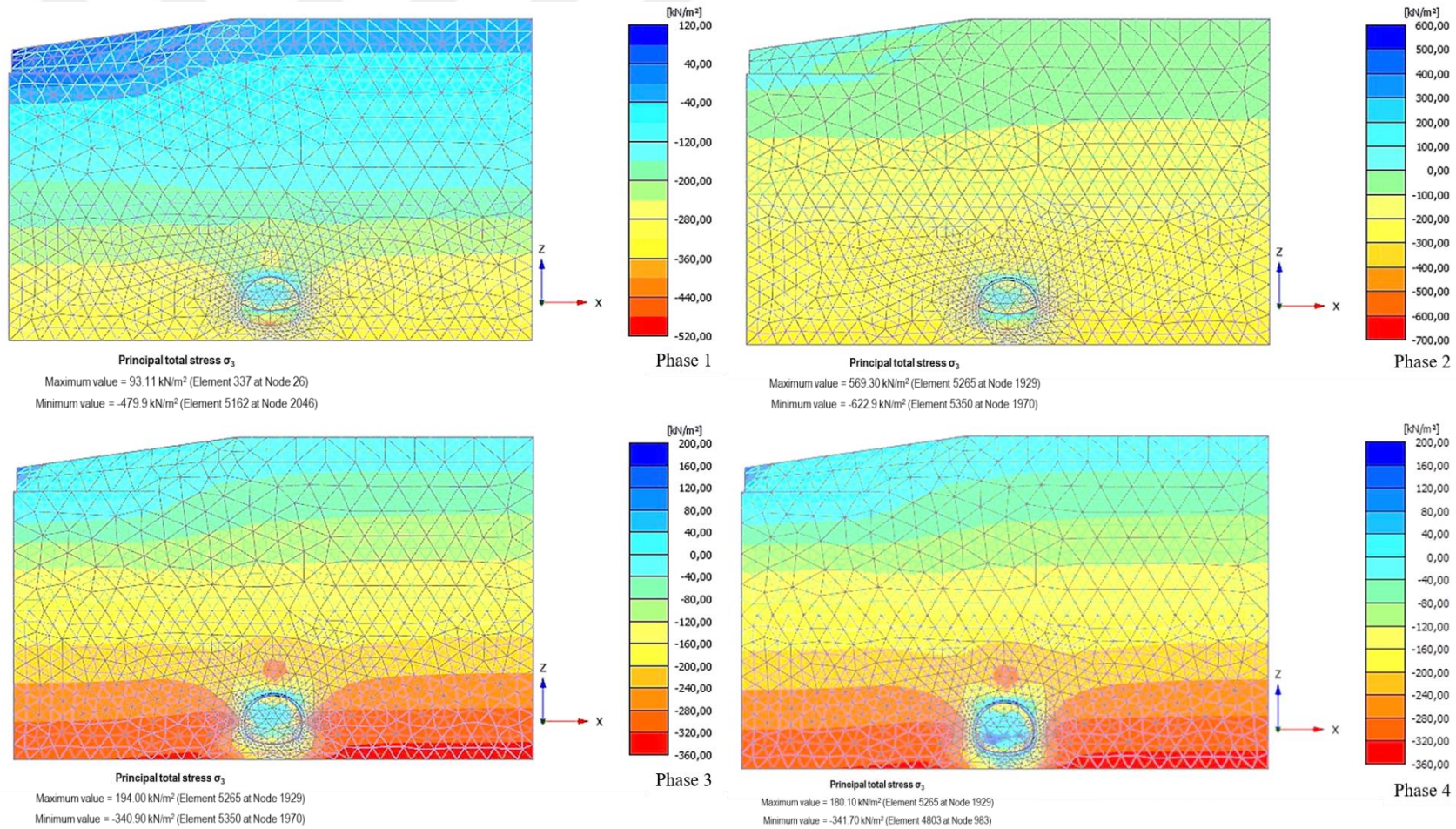


Figure 3.17. Principal stresses by phase for static loading case

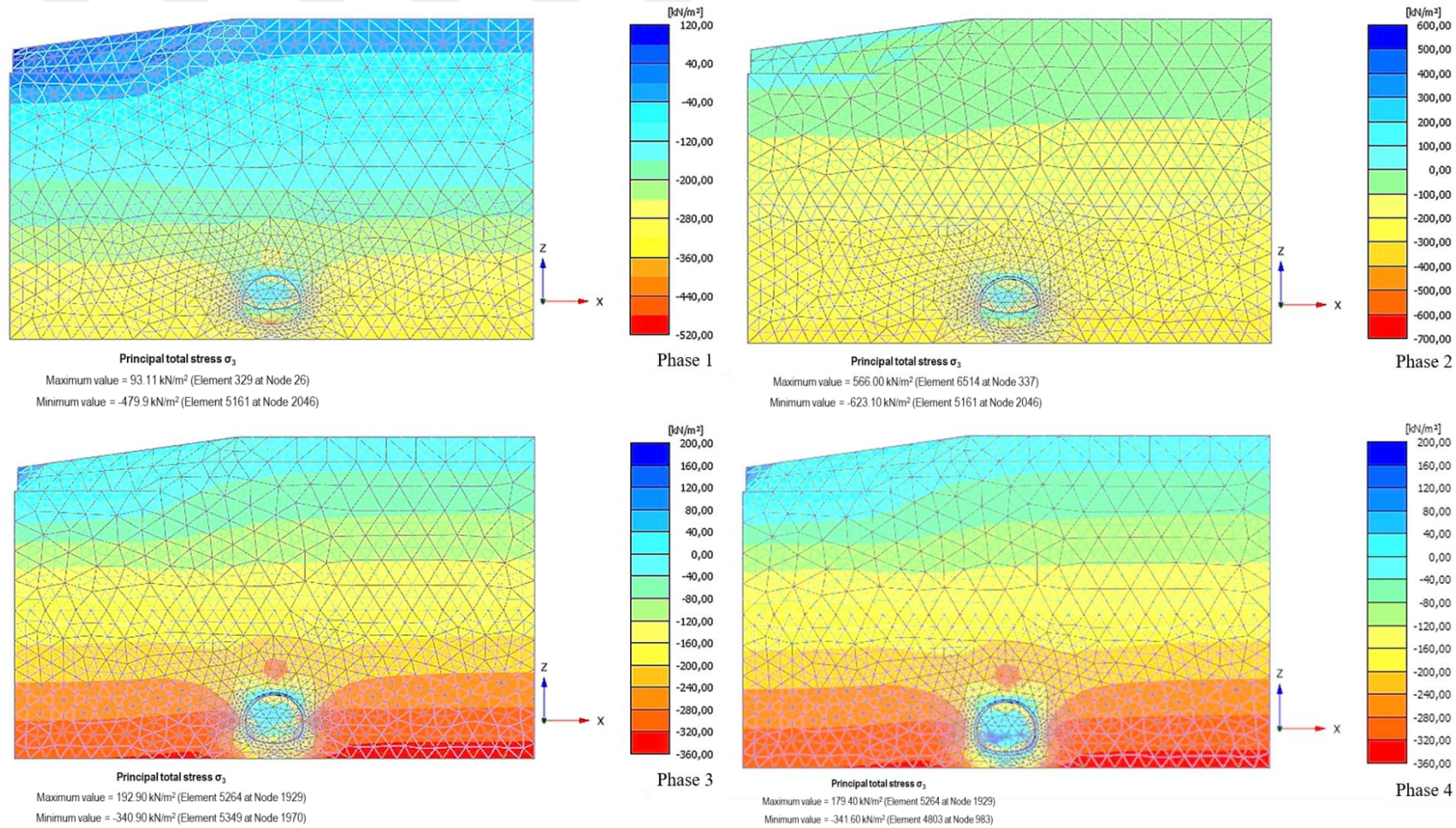


Figure 3.18. Principal stresses by phase for cyclic loading case (0.2 Hz)

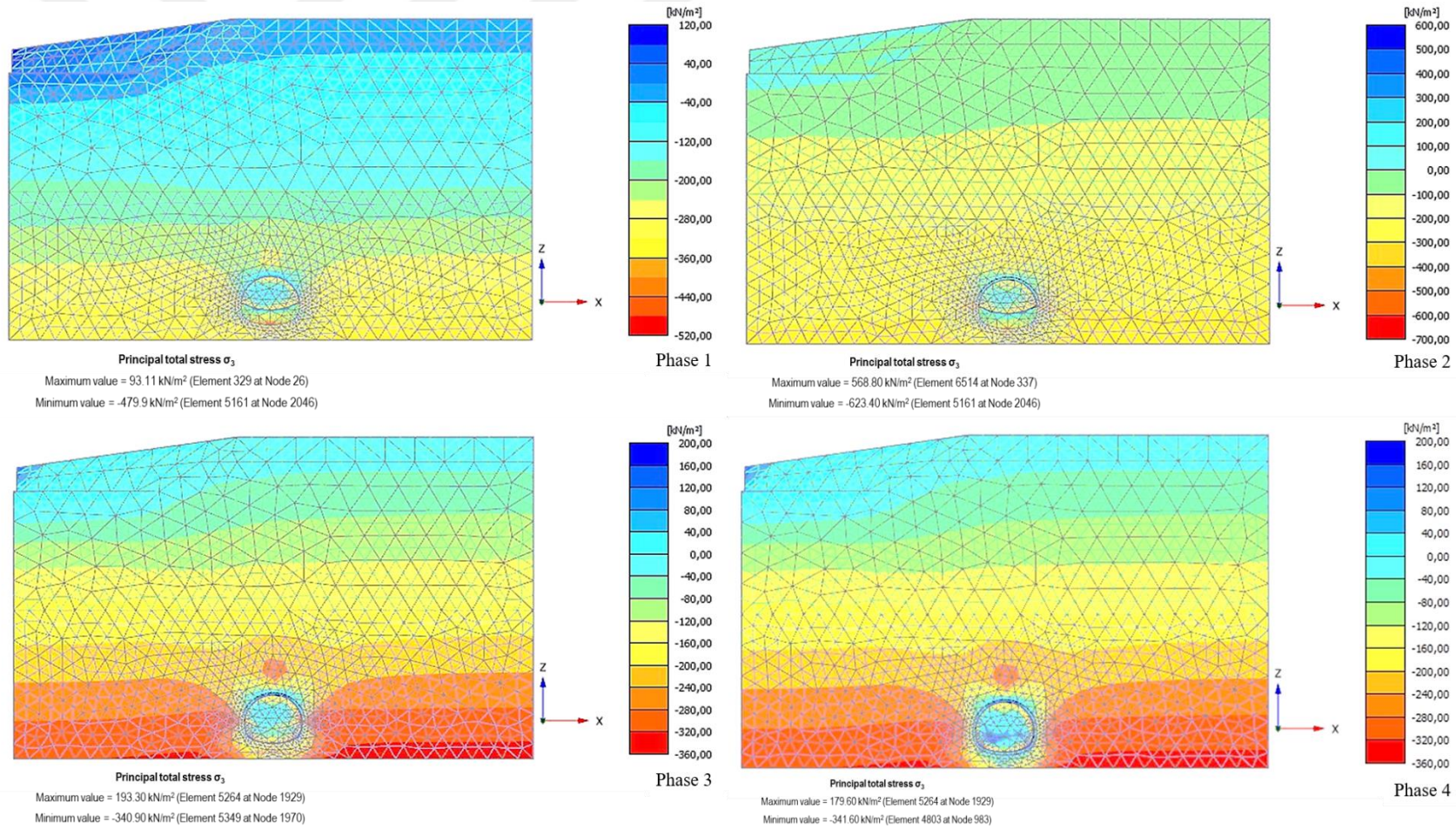


Figure 3.19. Principal stresses by phase for cyclic loading case (0.6 Hz)

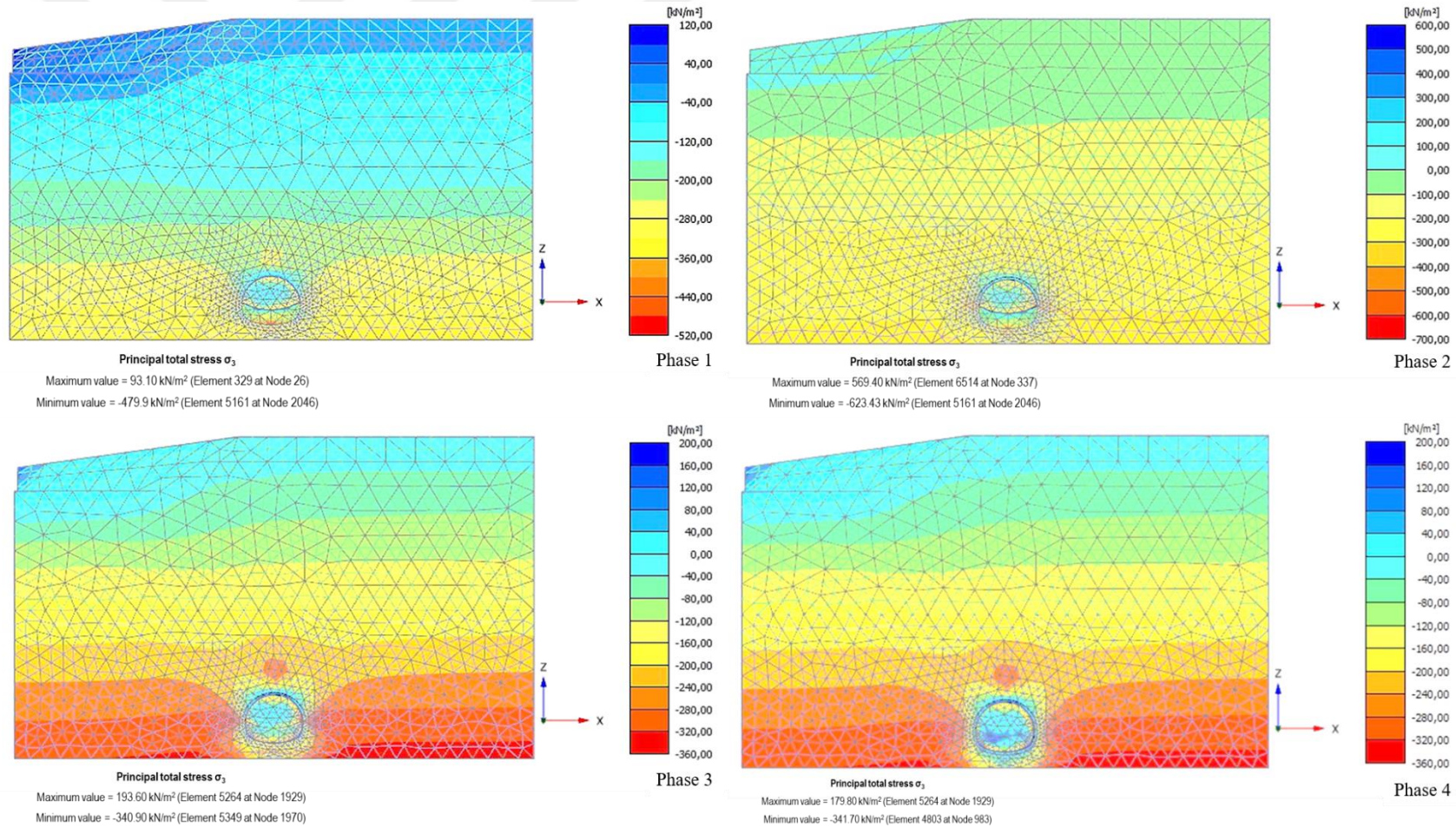
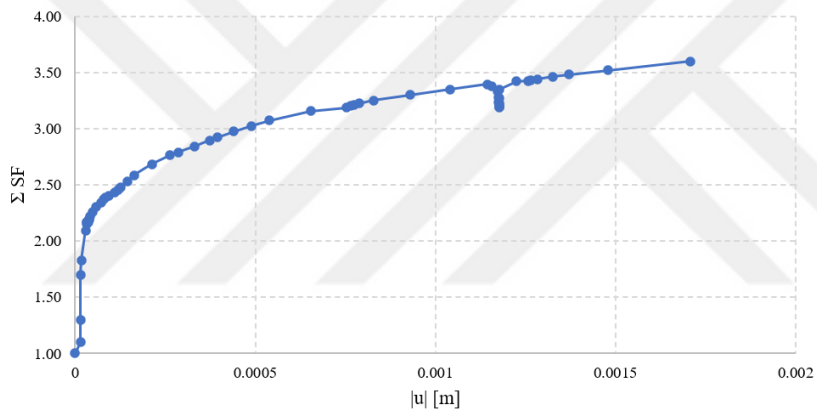
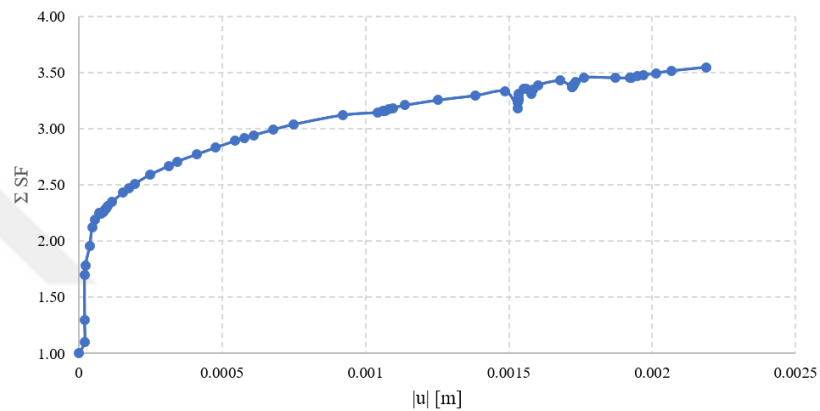


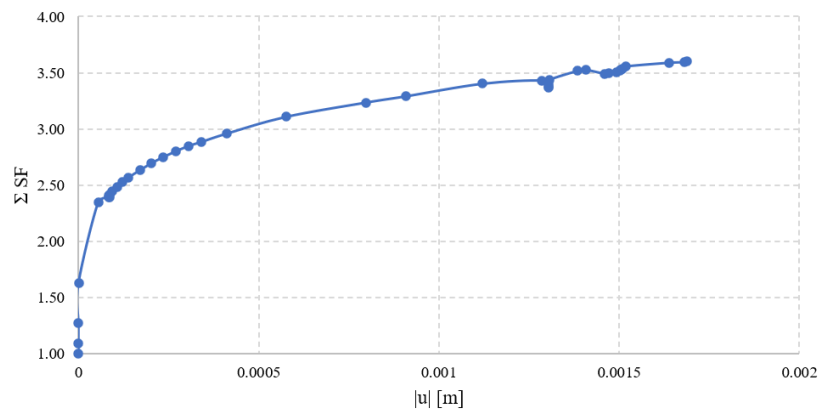
Figure 3.20. Principal stresses by phase for cyclic loading case (1.0 Hz)



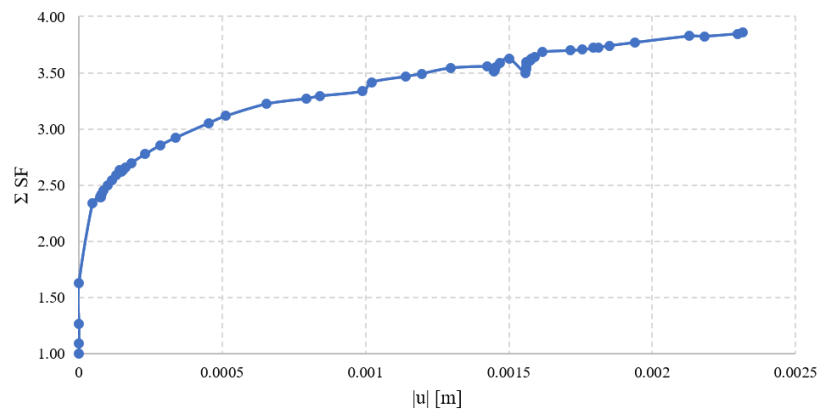
Safety factor curve for static loading case.



Safety factor curve for cyclic loading case (0.2 Hz).



Safety factor curve for cyclic loading case (0.6 Hz).



Safety factor curve for cyclic loading case (1.0 Hz).

Figure 3.21. Safety factor curves for static and cyclic loading cases

The results from the FEM simulation are summarized by Table 3.8 for total displacements, Table 3.9 for principal total stresses, and Table 3.10 case of the safety factors.

Table 3.8. Summary of the maximum total displacements,  $|u_{\max}|$ , units in mm

Phase	$ u_{\max} $ (Static)	$ u_{\max} $ (0.2 Hz)	$ u_{\max} $ (0.6 Hz)	$ u_{\max} $ (1.0 Hz)
1	1.140	1.524	1.388	1.276
2	1.873	2.496	2.276	2.093
3	1.901	2.535	2.310	2.124
4	1.919	2.558	2.332	2.144

Table 3.9. Summary of the principal total stresses,  $\sigma_3$ , units in  $\text{kN/m}^2$

Phase	Value	$\sigma_3$ (Static)	$\sigma_3$ (0.2 Hz)	$\sigma_3$ (0.6 Hz)	$\sigma_3$ (1.0 Hz)
1	Max. value	93.11	93.11	93.11	93.10
	Min. value	-479.90	-479.90	-479.90	-479.90
2	Max. value	569.30	566.00	568.80	569.40
	Min. value	-622.90	-623.10	-623.40	-623.30
3	Max. value	194.00	192.90	193.30	193.60
	Min. value	-340.90	-340.90	-340.90	-340.90
4	Max. value	180.10	179.40	179.60	179.80
	Min. value	-341.70	-341.60	-341.60	-341.70

Table 3. 10. Safety factors for static and cyclic loading scenarios

Value	SF (Static)	SF (0.2Hz)	SF (0.6Hz)	SF (1.0 Hz)
Max. value	3.60	3.55	3.60	3.86
Avg. value	2.76	2.90	2.90	3.10

## 4. DISCUSSION OF RESULTS

### 4.1. Comparative Analysis of the Loading Scenarios by Results

#### 4.1.1. $|u_{\max}|$ Assessment

$|u_{\max}|$  describes the maximum displacement in response to changes in each NATM tunnel phase. Since the ubiquitous gravity is acting in compression, each phase of the hypothetical NATM tunnel is also subjected to compressive stresses, which means displacement values in contraction. Figure 4.1 serves as an outline to represent the stresses acting on the NATM tunnel profile that is the same no matter the phase or type of loading scenario. This distribution is essential to figure out where the tunnel displacements are because the highest compression forces happen at the top of the excavation, meaning that  $|u_{\max}|$  is occurring on the roof of the structure, presenting small-displacement values that vary from 1.140 to 2.332 mm, as shown in Figure 4.2.

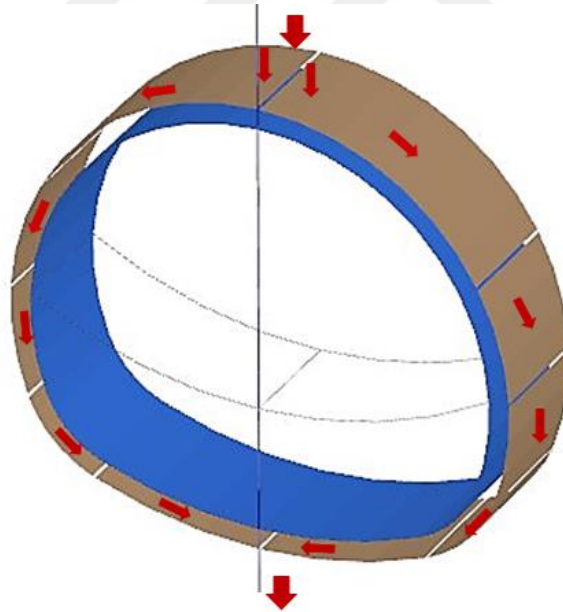


Figure 4.1. Stress distribution acting on the tunnel profile

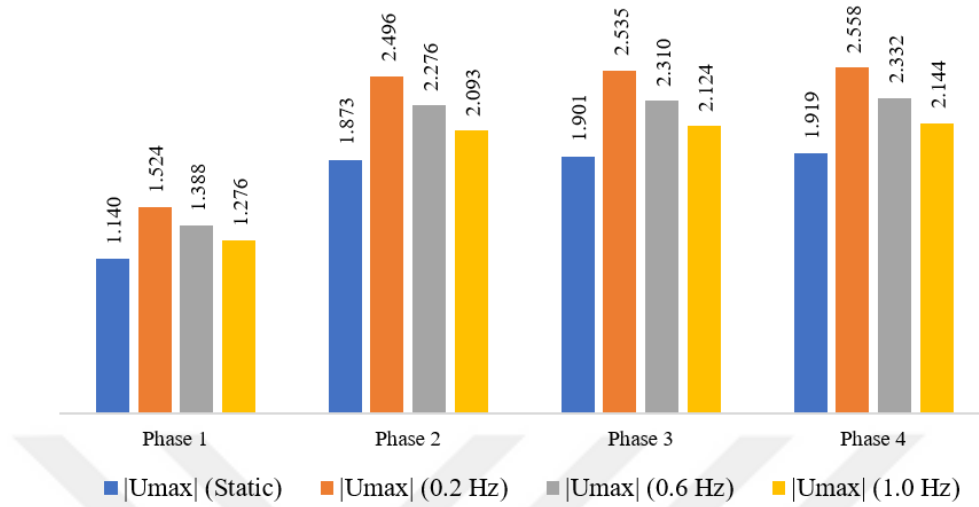


Figure 4.2. Maximum total displacements ( $|u_{\max}|$ ) per phase and scenario [mm]

Figure 4.2 compares how impacted an underground opening is for different loading scenarios, although  $|u_{\max}|$  assessment. The cyclic loading scenarios exhibit greater  $|u_{\max}|$  values than static load  $|u_{\max}|$  because a lower frequency value means a longer cycle time (Momeni et al., 2015). In other words, at a lower frequency, longer load application time, thus Bayburt tuff is more fatigued at a frequency of 0.2 Hz, which means a higher  $|u_{\max}|$ .

#### 4.1.2. $\Sigma_3$ Assessment

This section evaluates how the principal stresses (maximum and minimum) around the opening behave, as display in Figures 3.17, 3.18, 3.19, and 3.20. On the other hand, no significant changes have been observed in  $\sigma_3$  values per phase, as evidenced by Figure 4.3.



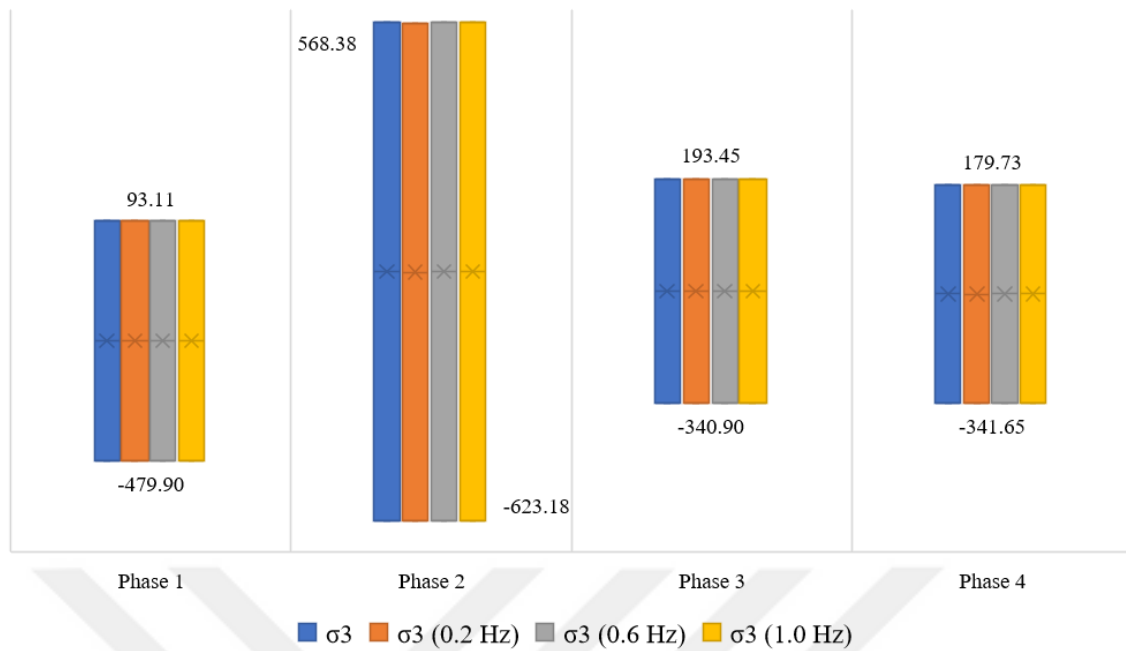


Figure 4.3. Maximum and minimum principal stresses per phase and scenario [kN/m<sup>2</sup>]

However, in the big picture, there are significant variations from one phase to the other; for instance, during Phase 1, no matter which loading scenario is, the hypothetical NATM tunnel undergoes 93.11 kN/m<sup>2</sup> and -479.90 kN/m<sup>2</sup> as  $\sigma_3$  maximum and minimum stresses, respectively; while in Phase 2 the underground opening undergoes 568.38 kN/m<sup>2</sup> and -623.18 kN/m<sup>2</sup>, which means that phase is subject to stresses of greater magnitude. Concerning the fatigue influence on  $\sigma_3$ , the Bayburt tuff responds with significant  $\sigma_3$  values for fewer frequencies. In other words, an inverse relationship between  $\sigma_3$  and frequency.

#### 4.1.3. SF Assessment

According to Belizario-Calsin et al. (2020), the security factor (SF) assesses the acting and resistant forces present in the excavation. PLAXIS 3D finite element software calculates the safety factor using phi/c reduction method that reduces the rock parameters until the rock collapses.

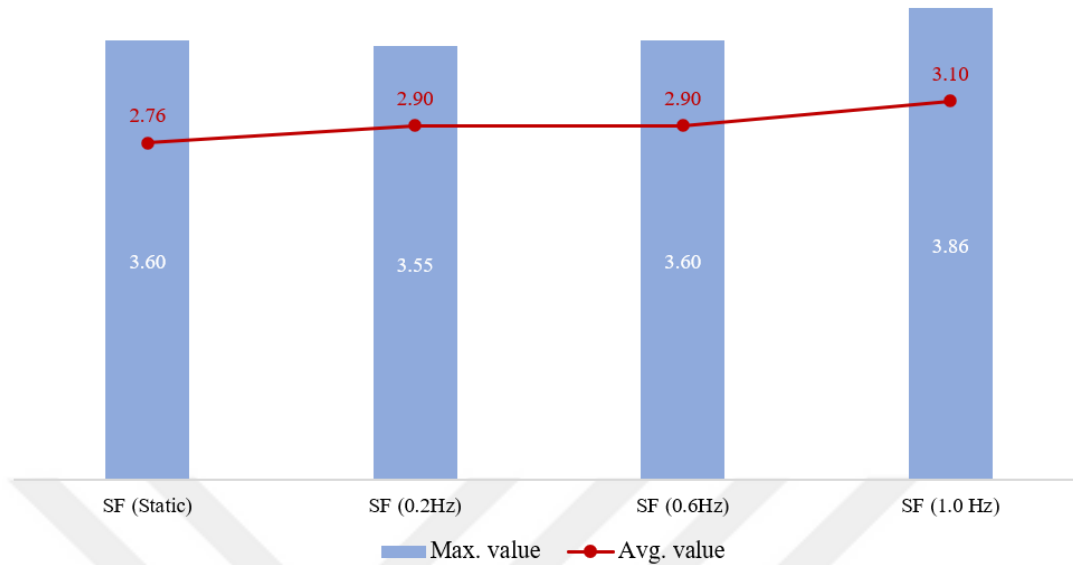


Figure 4.4. Safety factor (SF) per phase and scenario

Figure 4.4 compares both loading scenarios. On the one hand, the cyclic loading scenarios possess SF values higher values than the static loading case; nevertheless, all those scenarios present an  $SF > 1.5$ , which means that the hypothetical NATM tunnel is stable after the four phases. On the other hand, the fatigue effect is present through proportionality between frequency and SF because high frequencies mean shorter load application times (Beşer, 2017), increasing the Bayburt tuff strength. This statement is justified by Figure 4.5, where the laboratory results are compared for both static and cyclic loading cases.

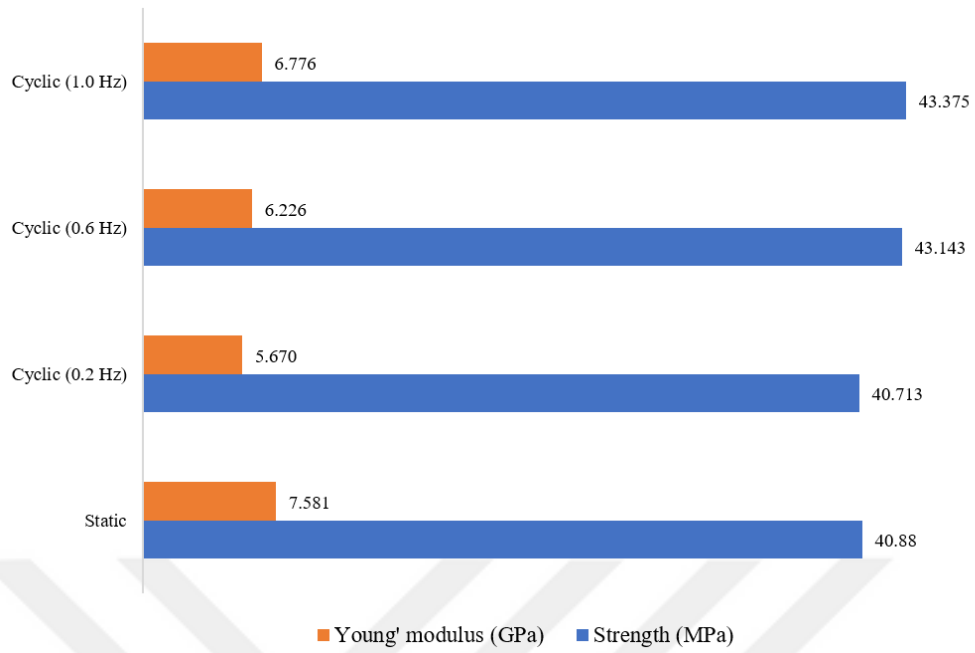


Figure 4.5. Scenario comparison based on  $\sigma_{ci}$  and E

## 5. CONCLUSIONS

This thesis shows the investigation results to analyze the effect of rock fatigue in designing a hypothetical NATM tunnel. The core value is to compare the static and cyclic loading scenarios by simulation, considering changes in frequency for cyclic loading case. The conclusions of this study are given below.

- i. There is a linear relationship between the fatigue effect and both strength and elasticity values in the Bayburt tuff. The cyclical strength values exceeded the static values from 0.6 Hz, while the static deformation modulus is more significant than those presented by the cyclical scenarios.
- ii. The cyclic loading scenarios exhibit greater  $|u_{\max}|$  values than static load  $|u_{\max}|$  because at a lower frequency, longer load application time, thus Bayburt tuff is more fatigued at a frequency of 0.2 Hz, which means a higher  $|u_{\max}|$ .
- iii. No significant changes have been observed in  $\sigma_3$  values per phase by comparing static and cyclic loading scenarios; nevertheless, there are significant variations from one phase to the other. It concluded that the Bayburt tuff responds with significant  $\sigma_3$  values for fewer frequencies. In other words, an inverse relationship between  $\sigma_3$  and frequency.
- iv. The two scenarios present a gradual linear increase from phase to phase, and this is visible in both  $|u_{\max}|$  and  $\sigma_3$  displayed in Table 3.9 and Table 3.10. However, for the cyclic loading case at lower frequency values, more significant magnitude deformations are reported than in the static scenario.
- v. The fatigue effect influence appears through proportionality between frequency and SF values because, compared with the static scenario, the cyclic develop higher values, which means a more stable structure.

Finally, the fatigue effect's influence on the Bayburt tuff, through variations in frequency, is demonstrated by comparing static and cyclic loading scenarios where different strength and elasticity values were obtained by the laboratory, leading to different results simulating a hypothetical NATM tunnel. This study leaves it pending for future researchers to complement the methodology described above with fieldwork to achieve values close to reality.

## 6. REFERENCES

- Alves Filho, A., 2007. Elementos Finitos—A base da tecnologia CAE, São Paulo Editora: Érica, Brazil
- Annicchini, M., 2019. Fadiga em Rochas Intactas, Revista Científica Semana Acadêmica, 1, Brazil.
- A.S.T.M., 2000. Standard Terminology Relating to Fatigue and Fracture, E1823-20a, West Conshohocken, Pennsylvania.
- Aydiner, K., 2001. Decision support system approach for cut-and-fill mining, Doctoral Thesis, O.T.Ü., Fen Bilimleri Entitüsü, Ankara.
- Bagde, M. N. and Petroš, V., 2005. Waveform effect on fatigue properties of intact sandstone in uniaxial cyclical loading, Rock mechanics and rock engineering, 38, 3, 169-196, Austria.
- Beer, F. P., Johnston, E. R., DeWolf, J. T. and Mazurek, D. F., 2015. Mechanics of Materials, McGraw-Hill Education Ltd, Seventh Edition, New York, United States.
- Belizario-Calsin, M., et al., 2020. Empirical and Numerical Finite-Element-Based Model to Improve Narrow Vein Mine Design in Peruvian Mining, In IOP Conference Series: Materials Science and Engineering, 758, 1, 012014, Sanya.
- Beşer M. H., 2017. Tekrarlı Yüklemenin Tefrit Kayacının Dayanımı Üzerindeki Etkisi, Yüksek Lisans Tezi, K.T.Ü., Fen Bilimleri Enstitüsü, Trabzon.
- Beşer, M. H. and Aydiner, K., 2018. The Effect of Loading Cycles on The Uniaxial Compressive Strength of The Rock Under Cyclic Loading, KAYAMEK'2018 12. BÖLGESEL KAYA MEKANİĞİ SEMPOZYUMU, 59-61, Trabzon, Turkey.
- Boidy, E., Bouvard, A. and Pellet, F., 2002, Back analysis of time-dependent behaviour of a test gallery in claystone, Tunnelling and Underground Space Technology, 17, 4, 415-424.
- Brady, B. H. and Brown, E. T., 2004. Rock mechanics: for underground mining, Kluwer Academic Publishers, Third Edition, New York.
- Cerfontaine, B. and Collin, F., 2018. Cyclic and fatigue behaviour of rock materials: review, interpretation and research perspectives, Rock Mechanics and Rock Engineering, 51, 2, 391-414, Austria.
- Deere, D. U. and Miller, R. P., 1966. Engineering classification and index properties for intact rock, Illinois Univ At Urbana Dept Of Civil Engineering, Illinois.
- Demir, K., and Özbayir, T., 2016. Design and Back Analysis of NATM Tunnels in Fractured Rock, Paper presented at the ISRM International Symposium - EUROCK 2016, Ürgüp, Turkey.

- Erarslan, N. and Ghamgosar, M., 2014. Fracturing and indirect tensile strength of brittle and ductile rocks, In ISRM Regional Symposium-EUROCK 2014, Vigo, Spain.
- Fasihnikoutalab, M. H., et al., (2012). Numerical stability analysis of tunnel by PLAXIS, EJGE, 17, 451-461.
- Schokking, F., 2011. Luis I. González de Vallejo, Mercedes Ferrer: Geological Engineering, Bulletin of Engineering Geology and the Environment, 70, 3, 529-530.
- Gundewar, S. C., 2014. Application of rock mechanics in surface and underground mining. Indian Bureau of Mines, 165.
- Hoek, E. and Brown, E. T., 2019. The Hoek–Brown failure criterion and GSI–2018 edition, Journal of Rock Mechanics and Geotechnical Engineering, 11, 3, 445-463.
- Hoek, E. and Diederichs, M. S., 2006. Empirical estimation of rock mass modulus, International journal of rock mechanics and mining sciences, 43, 2, 203-215.
- Hoek, E., Carranza-Torres, C. and Corkum, B., 2002. Hoek-Brown failure criterion-2002 edition. Proceedings of NARMS-Tac, 1, 1, 267-273.
- Hawkins, A.B., 2009. Ulusay, R., Hudson, J. A. (eds.): The Complete ISRM Suggested Methods for Rock Characterisation, Testing and Monitoring, Bull Eng Geol Environ 68, 287–288.
- Leiva, E., 2013. Characterization of the Zeolite from the Quinamávida Tuffs, Master's Thesis. Universidad Católica de la Santísima Concepción, Chile.
- Li, D., and Wong, L. N. Y., 2013. The Brazilian disc test for rock mechanics applications: review and new insights. Rock mechanics and rock engineering, 46, 2, 269-287.
- Manouchehrian, A. and Cai, M., 2017. Analysis of rockburst in tunnels subjected to static and dynamic loads. Journal of Rock Mechanics and Geotechnical Engineering, 9, 6, 1031-1040.
- Marinos, P. and Hoek, E., 2000. GSI: a geologically friendly tool for rock mass strength estimation. In ISRM international symposium, Melbourne, Australia.
- Momeni, A., Karakus, M., Khanlari, G. R. and Heidari, M., 2015. Effects of cyclic loading on the mechanical properties of a granite, International Journal of Rock Mechanics and Mining Sciences, 100, 77, 89-96.
- Pellet, F., Roosefid, M. and Deleruyelle, F., 2009. On the 3D numerical modelling of the time-dependent development of the damage zone around underground galleries during and after excavation, Tunnelling and Underground Space Technology, 24, 6, 665-674.

- Plaxis bv, PLAXIS 3D 2017 Material Models Manual.  
<https://communities.bentley.com/products/geotech-analysis/w/plaxis-soilvision-wiki/46137/manuals---plaxis> 01 Ocak 2020
- Plaxis bv, PLAXIS 3D 2017 Tutorial Manual.  
<https://communities.bentley.com/products/geotech-analysis/w/plaxis-soilvision-wiki/46137/manuals---plaxis> 01 Ocak 2020
- Plaxis bv, PLAXIS 3D 2017 Reference Manual.  
<https://communities.bentley.com/products/geotech-analysis/w/plaxis-soilvision-wiki/46137/manuals---plaxis> 01 Ocak 2020
- Rossmannith, H. P., 2014. Rock fracture mechanics, Springer, 275, Austria.
- Shen, B., Stephansson, O. and Rinne, M., 2014. Modelling rock fracturing processes. A Fracture Mechanics Approach Using FRACOD, Springer Dordrecht Heidelberg, New York, London.
- Singh, S. K., 1989. Fatigue and strain hardening behaviour of graywacke from the flagstaff formation, Engineering Geology, 26, 2, 171-179, New South Wales.
- Solans, D., Hormazábal, C., Rojas, B. and León, R., 2015. Comparación de tres metodologías de análisis sísmico de túnel NATM en suelos finos de Santiago. Obras y proyectos, 17, 14-21.
- Song, Y., Wang, H. and Ren, M., 2019. Experimental study on deformation and failure characteristics of discontinuous prefabricated fractured tuff, Journal of Geophysics and Engineering, 16, 5, 862-874.
- Swoboda, G., Marencic, M. and Mader, I., 1994. Finite element modelling of tunnel excavation. International Journal of Engineering Modelling, 6, 51-63, Austria.
- Su, G., Hu, L., Feng, X. et al., 2018. True Triaxial Experimental Study of Rockbursts Induced By Ramp and Cyclic Dynamic Disturbances. Rock Mechanics and Rock Engineering 51, 4, 1027–1045.
- Su, G., Feng, X., Wang, J. et al., 2017. Experimental Study of Remotely Triggered Rockburst Induced by a Tunnel Axial Dynamic Disturbance Under True-Triaxial Conditions. Rock Mechanics and Rock Engineering 50, 2207–2226.
- URL-1, [www.communities.bentley.com](http://www.communities.bentley.com), Hoek-brown mobilized dilatancy evolution, 13 December 2020.
- Ván P. and Vásárhelyi B., 2013. Sensitivity analysis of the generalized Hoek-Brown failure criterion. ISRM International Symposium - EUROCK 2013, Wroclaw.
- Wang, H., Chang, T. P. and Hung, J. J., 2010. Determining the cyclic strength of geomaterials under low frequency cyclic loading with acoustic emission, Journal of Marine Science and Technology, 18, 6, 837-847.

Wang, Z., Li, S., Qiao, L. and Zhang, Q., 2015. Finite element analysis of the hydro-mechanical behavior of an underground crude oil storage facility in granite subject to cyclic loading during operation, International Journal of Rock Mechanics and Mining Sciences, 73, 70-81.

Zhu, B., 2018. The Finite Element Method: Fundamentals and Applications in Civil, Hydraulic, Mechanical and Aeronautical Engineering. John Wiley & Sons Singapore Pte. Ltd., Singapore.

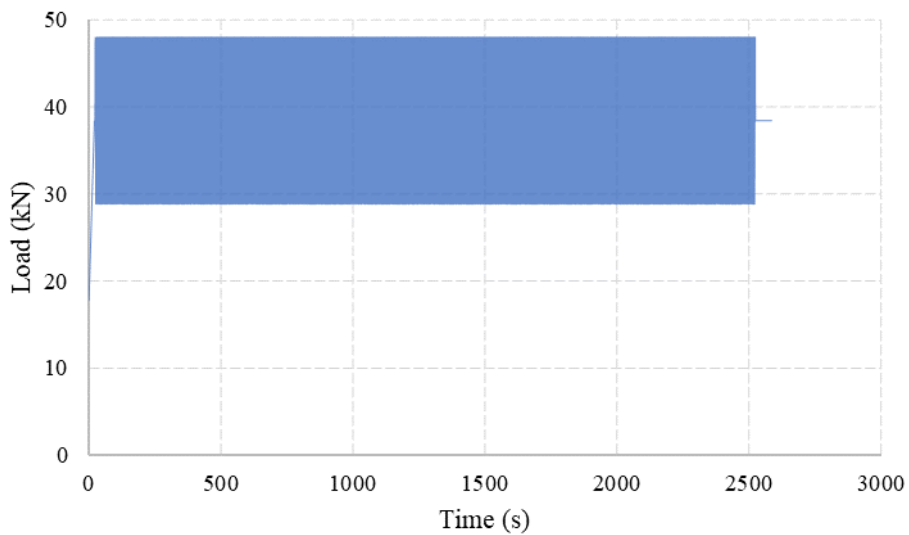




## 7. ANNEXES

### Uniaxial Cyclic Loading Test

Laboratory Name: KTU Mining Engineering Department  
Number of Specimen: B-UF-1-2  
Specimen Name: Bayburt Tuff  
Load Range: 30 – 50%  
Frequency: 0.2 Hz  
Number of Cycles: 500



Max. Load	Max. Stress	Duration	Min. Load
48.040 kN	21.16 MPa	2585.85 s	17.804 kN

Annex 1. Cyclic loading report for Bayburt tuff specimen UF 1-2 (0.2 Hz)

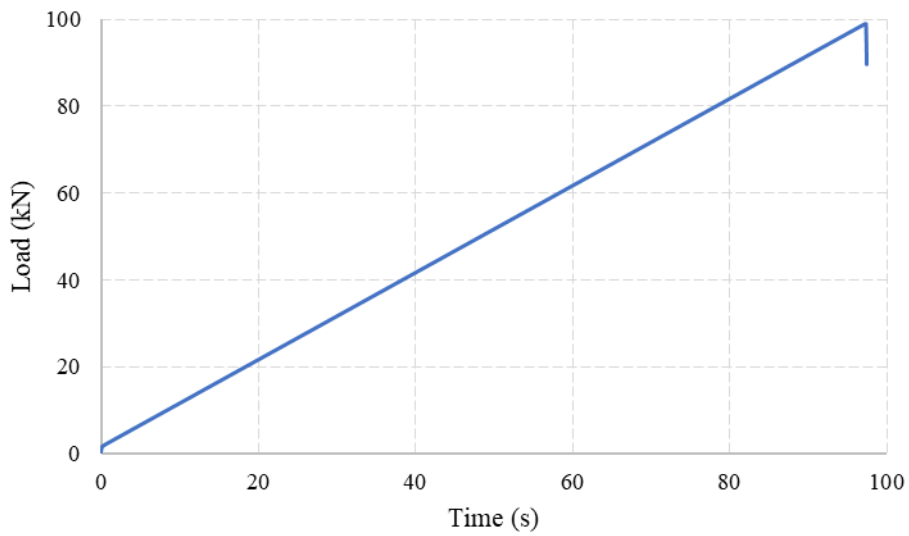
### Uniaxial Compressive Strength Test

Laboratory Name: KTU Mining Engineering Department

Number of Specimen: B-UF-1-2

Specimen Name: Bayburt Tuff

Type of Test: Uniaxial Compressive Strength Test After Cyclic Loads



Max. Load	Max. Stress	Duration
98.922 kN	43.56 MPa	97.50 s

Annex 2. Uniaxial compression strength report after cyclic loads for Bayburt tuff specimen UF 1-2 (0.2 Hz)

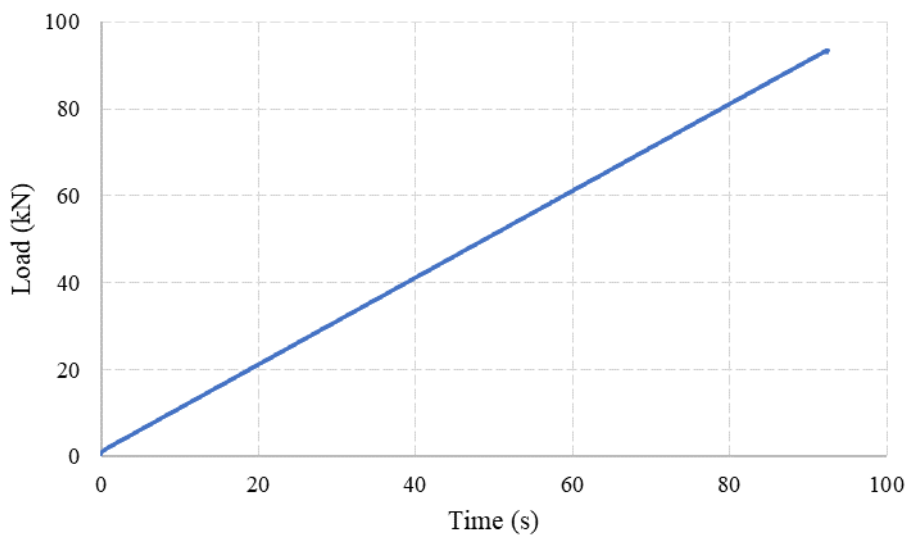
### Uniaxial Compressive Strength Test

Laboratory Name: KTU Mining Engineering Department

Number of Specimen: B-UF-1-3

Specimen Name: Bayburt Tuff

Type of Test: Uniaxial Compressive Strength Test After Cyclic Loads



Max. Load	Max. Stress	Duration
93.40 kN	41.20 MPa	92.50 s

Annex 3. Uniaxial compression strength report after cyclic loads for Bayburt tuff specimen  
UF 1-3 (0.2 Hz)

### Uniaxial Cyclic Loading Test

Laboratory Name: KTU Mining Engineering Department

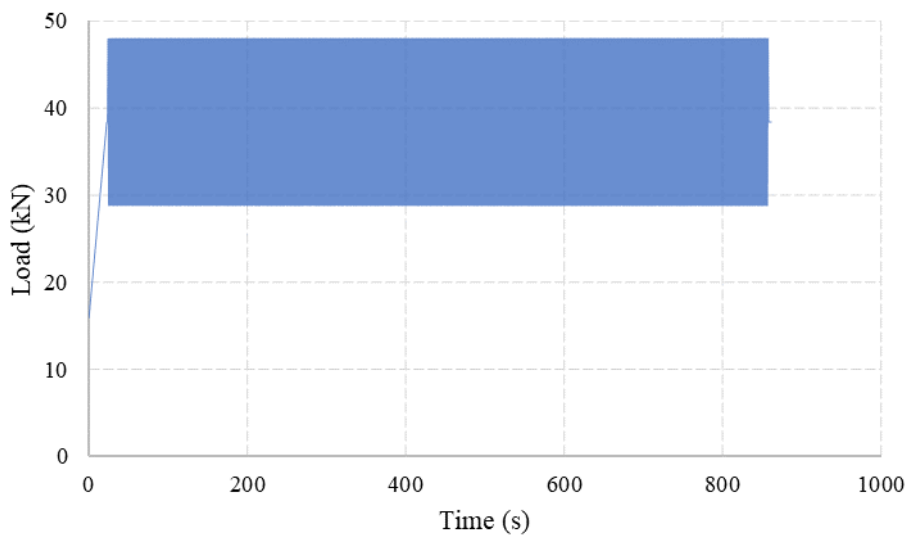
Number of Specimen: B-UF-2-1

Specimen Name: Bayburt Tuff

Load Range: 30 – 50%

Frequency: 0.6 Hz

Number of Cycles: 500



Max. Load	Max. Stress	Duration	Min. Load
48.035 kN	21.13 MPa	861.50 s	15.941 kN

Annex 4. Cyclic loading report for Bayburt tuff specimen UF 2-1 (0.6 Hz)

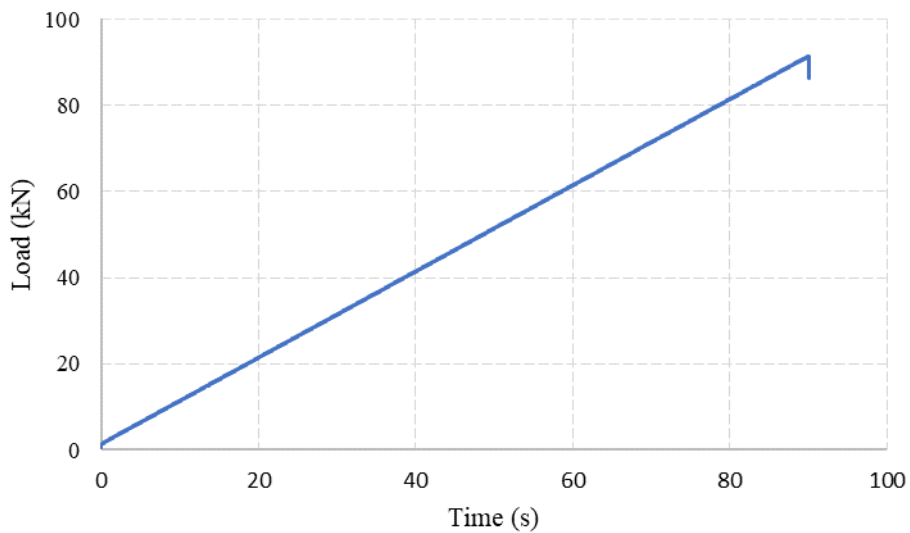
### Uniaxial Compressive Strength Test

Laboratory Name: KTU Mining Engineering Department

Number of Specimen: B-UF-2-1

Specimen Name: Bayburt Tuff

Type of Test: Uniaxial Compressive Strength Test After Cyclic Loads



Max. Load	Max. Stress	Duration
91.361 kN	40.19 MPa	90.15 s

Annex 5. Uniaxial compression strength report after cyclic loads for Bayburt tuff specimen UF 2-1 (0.6 Hz)

### Uniaxial Cyclic Loading Test

Laboratory Name: KTU Mining Engineering Department

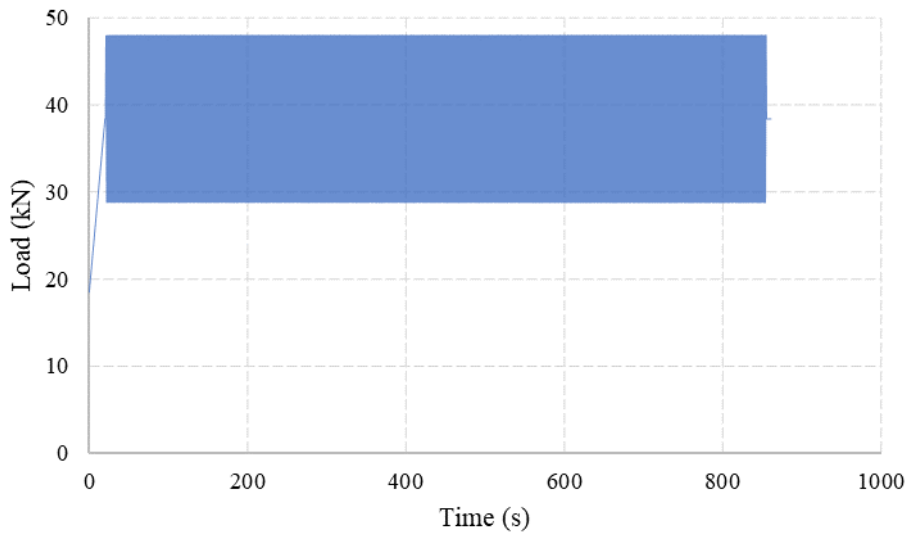
Number of Specimen: B-UF-2-2

Specimen Name: Bayburt Tuff

Load Range: 30 – 50%

Frequency: 0.6 Hz

Number of Cycles: 500



Max. Load	Max. Stress	Duration	Min. Load
48.025 kN	21.13 MPa	860.95 s	18.489 kN

Annex 6. Cyclic loading report for Bayburt tuff specimen UF 2-2 (0.6 Hz)

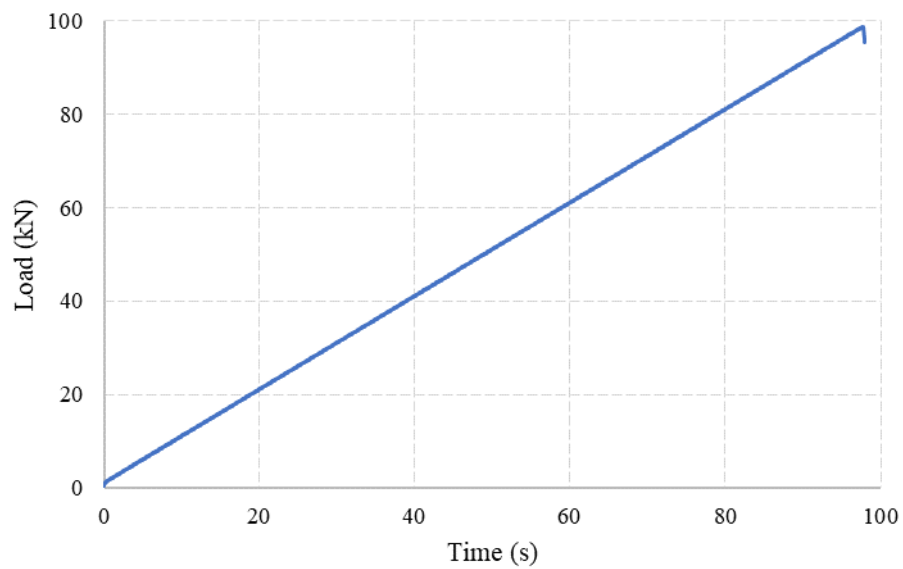
### Uniaxial Compressive Strength Test

Laboratory Name: KTU Mining Engineering Department

Number of Specimen: B-UF-2-2

Specimen Name: Bayburt Tuff

Type of Test: Uniaxial Compressive Strength Test After Cyclic Loads



Max. Load	Max. Stress	Duration
98.823 kN	43.49 MPa	97.90 s

Annex 7. Uniaxial compression strength report after cyclic loads for Bayburt tuff specimen UF 2-2 (0.6 Hz)

## Elasticity and Cyclic Loading test

Laboratory Name: KTU Mining Engineering Department

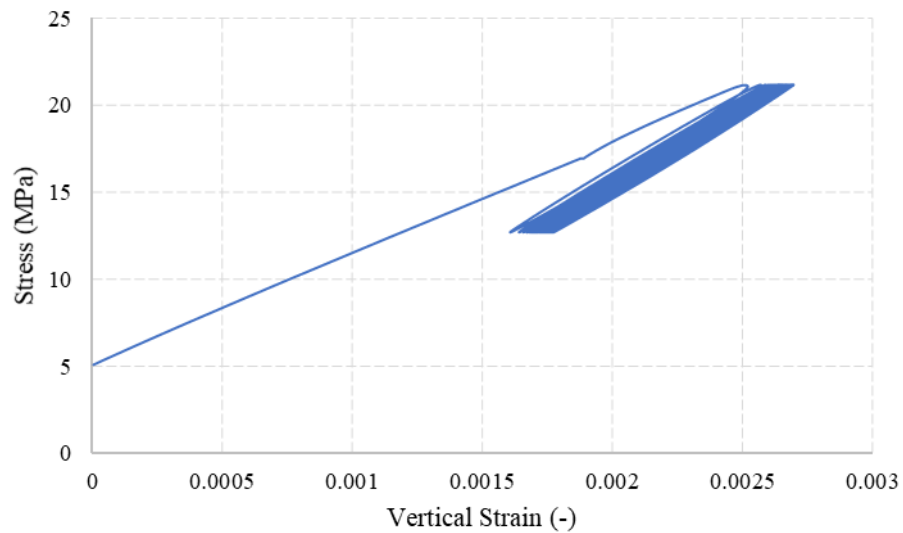
Number of Specimen: B-UF-2-3

Specimen Name: Bayburt Tuff

Load Range: 30 – 50%

Frequency: 0.6 Hz

Number of Cycles: 500



Max. Load	Max. Stress	Duration	Min. Load
48.037 kN	21.18 MPa	1070.79 s	16.420 kN
Ranged E Modulus			
6225.61 MPa			

Annex 8. Report about stress-strain curve and cyclic loading test for Bayburt tuff specimen UF 2-3 (0.6 Hz).



## **BIOGRAPHY**

Pontifical Catholic University of Peru in 2016. In 2018, he started his master studies at Karadeniz Technical University in mining engineering. He has professional experience in underground mining and rock mechanics investigation, with a particular interest in rock mechanics applications and research, continuous improvement and optimization through statistic application, and costs and valuations. Besides, possess English, Portuguese, Spanish, and Turkish language knowledge.

